CR-166265
(NASA)
SQT

STUDY OF RADIATIVELY SUSTAINED CESIUM PLASMAS FOR SOLAR ENERGY CONVERSION

By A.J. Palmer and G.J. Dunning

July 1980

(NASA-CR-166265) STUDY OF RADIATIVELY SUSTAINED CESIUM PLASMAS FOR SOLAR ENERGY CONVERSION Final Report, 1 Jul. 1978 - 30 Jun. 1980 (Hughes Research Labs.) 67 p
HC A04/MF A01

N82-13039

CSCL 10A G3/92

Unclas
02609

HUGHES RESEARCH LABORATORIES
1311 Malibu Canyon Road
Malibu, California 90265

for

AMES RESEARCH CENTER
NATIONAL AERONAUTICS AND SPACE ADMINISTRATION

TECHNICAL REPORT STANDARD TITLE PAGE

1. Report No.	2. Government Accession No.	3. Recipient's Catalog No.

4. Title and Subtitle
STUDY OF RADIATIVELY SUSTAINED CESIUM PLASMAS FOR SOLAR ENERGY CONVERSION

5. Report Date
July 1980

6. Performing Organization Code

7 Author(s)
A.J. Palmer and G.J. Dunning

8. Performing Organization Report No.

9. Performing Organization Name and Address
Hughes Research Laboratories
3011 Malibu Canyon Road
Malibu, California 90265

10. Work Unit No.

11. Contract or Grant No.
NAS 2-10001

12. Sponsoring Agency Name and Address
Ames Research Center
National Aeronautics and Space Administration

13. Type of Report and Period Covered
Final Report
1 Jul 1978-30 Jun 1980

14. Sponsoring Agency Code

15. Supplementary Notes
Point of contact: Richard Dahms M/S 230-3, Ames Research Center
Moffett Field, CA. (415) 965-5408 or FTS 448-5408

16. Abstract
The results of a two-year experimental and theoretical study aimed at developing a novel high-temperature solar electric converter are reported. The converter concept is based on the use of an alkali plasma to serve as both an efficient high-temperature collector of solar radiation as well as the working fluid for a high-temperature working cycle. The working cycle is a simple magneto-hydrodynamic (MHD) Rankine cycle employing a solid electrode Faraday MHD channel. The motivation for developing this type of solar electric converter is based primarily on the cost and weight reduction premiums for operating a space solar electric generator at the maximum possible temperature. Several research milestones have been attained on this program toward the goal of developing such a generator. These include the construction of a theoretical model for coupling sunlight in a cesium plasma and the experimental demonstration of cesium plasma heating with a solar simulator in excellent agreement with the theory. Analysis of a solar MHD working cycle in which excimer laser power rather than electric power is extracted is also presented. The analysis predicts a positive gain coefficient on the Cs-Xe excimer laser transition.

17. Key Words (Selected by Author(s))
Solar electric converters
Solar sustained plasmas
Solar pumped lasers

18. Distribution Statement
Unlimited

STAR Category 92

19. Security Classif. (of this report)	20. Security Classif. (of this page)	21. No. of Pages	22. Price*
UNCLASSIFIED	UNCLASSIFIED	67	

*For sale by the Clearinghouse for Federal Scientific and Technical Information, Springfield, Virginia 22151.

TABLE OF CONTENTS

LIST OF ILLUSTRATIONS

SECTION 1

INTRODUCTION

In converting solar radiation to electric power in space, there is a high premium on the ability of the converter to operate at high temperature. There are two fundamental reasons for this. First, higher operating temperatures permit using a higher concentration ratio for the incident solar radiation. This favorably affects the cost and weight of large systems since the cost and weight of the concentrator per unit surface area are generally less than those of the collector. Second, operating the converter at high temperature permits using smaller radiators for rejecting the waste heat. (The radiator is typically the heaviest component of projected space power systems.) These premiums on high temperature apply to solar electric converters in general. In the heat-engine approach to solar electric conversion, there is the additional advantage that the working cycle efficiency is higher at higher temperatures.

This report presents the results of a two-year study aimed at developing an ultra-high-temperature solar electric heat engine converter. In the converter concept, an alkali plasma serves as both an efficient high-temperature collector of solar radiation as well as the working fluid for a high-temperature working cycle. The working cycle is a simple magneto-hydrodynamic (MHD) Rankine cycle employing a solid electrode Faraday MHD channel.

The simplest and most attractive solar-powered MHD cycle for high-power ($\gtrsim$10 kW) solar electric converters in space is a plasma-phase MHD converter utilizing a pure alkali Rankine cycle. Solar radiation concentrated by a factor of several thousand would heat cesium or potassium to $\sim$3000°K at a pressure of about 10^3 Torr. The hot plasma would flow through a nozzle and across an $\sim$10-kG magnetic field, thereby driving an electrical current transverse to the flow direction. At the above temperature and pressure, a pure cesium plasma will have a high enough electrical conductivity to enable electric power to be extracted efficiently from the plasma with a simple Faraday MHD channel employing

solid electrodes.[1] The plasma would remain sufficiently conductive to extract power in this way down to a temperature of ∿1800°K. The net cycle efficiency is expected to be ∿15%,[1] and, at a 1000°K condensor temperature, the reject heat can be radiated away at a rate per unit radiator area of ∿60 kW/m^2.

An alternative to radiating away the reject heat from the plasma MHD cycle would be to use the reject heat to drive a liquid-metal MHD bottoming cycle. The projected efficiency of one liquid-metal MHD cycle operating between 300 and 1000°K is calculated to be ∿60%.[2] Such a binary cycle could retain the simplicity, ruggedness, and relative inexpensiveness of MHD and would operate with an overall efficiency of ∿66%, but it would do so at the expense of requiring a considerably higher radiator area in spite of the higher efficiency because of the fourth-power dependence of the radiation rate on temperature.

The above approach to space solar power was originated independently by Hughes Research Laboratories (HRL)[3] and by the University of Washington's Aerospace and Energetics Center[4] about two years ago. We have achieved during those two years three major milestones towards the realization of this type of converter. First, we formulated a complete and versatile theoretical model of the physics of coupling solar radiation to a cesium plasma. The model, in the form of a computer program, treats a variety of experimental conditions and is easily adapted to treat the other alkalies.[5] Second, we have considered in some detail three MHD working cycles: plasma MHD using a single alkali species cycle;[1] two-phase liquid-metal MHD using either a single or two alkali species cycle;[2] and an alkali rare gas (Cs-Xe) plasma, MHD cycle in which excimer laser power is extracted in place of electric power.[6] Finally, we recently demonstrated heating of a cesium plasma in a laboratory experiment using a solar simulator light source.[7] The measured temperature of the plasma was within 20% of that predicted by our theoretical model for the conditions of the experiment.

The major theoretical and experimental research milestones attained to date on this program are presented in Sections 2 and 3. Important research objectives remain for establishing firmly the feasibility of this concept for space solar power, and these are discussed in Section 4.

SECTION 2

THEORETICAL PROGRAM

A. IDENTIFICATION OF HIGH-TEMPERATURE COLLECTOR

To achieve highest efficiency in the heat-engine approach to solar-electric conversion, it is advantageous to deposit the solar radiation into the working fluid at as high a temperature as possible. For this temperature to approach the upper limit of the sun's temperature, the radiation must be absorbed directly in the working fluid in a plasma state. Therefore, a plasma in the temperature range of 3000 to 6000°K needs to be identified that presents a broadband absorption cross section throughout the solar spectrum that is large enough to permit using moderate densities and dimensional scales for efficient coupling of the radiation to the plasma.

The primary sources of broadband absorption of visible radiation in plasmas are inverse bremsstrahlung (free-free electron transitions) and photo-ionization (bound-free electron transitions). If one assumes thermal ionization, as described by Saha's equation, then the absorption cross section (per ground state) caused by free-free transitions in a hydrogen-like plasma is[8]

$$\sigma_{ff} = \left(7.9 \cdot 10^{-18}\right)\left(\frac{V_I}{h\nu}\right)^3 \frac{\exp(-V_I/T)}{2(V_I/T)} \text{ cm}^2 \quad , \tag{1}$$

where V_I is the ionization potential, T is the plasma temperature, and $h\nu$ is the photon energy. At a temperature near 5000°K, even with a low ionization potential species, the cross section is quite small; therefore, very high densities and associated high plasma pressures will be needed to obtain a practical value for the free-free absorption coefficient in the solar spectrum ($h\nu \simeq 1$ to 3 eV).

On the other hand, the absorption cross section caused by bound-free transitions can be much larger in the visible than the free-free transition cross section. Combining Kramer's formula for the hydrogenic bound-free cross section per excited state with an assumed Boltzmann

distribution for the excited state population yields the cross section per ground state as[8]

$$\sigma_{bf} = \left(7.9 \cdot 10^{-18}\right)\left(\frac{V_I}{h\nu}\right)\left(\sum_1^{\infty} \frac{(2L(i) + 1)}{n^*(i)^3}\right) \exp\left(\frac{E(i) - V_I}{T}\right) \quad , \qquad (2)$$

where $n^*(i)$ is the effective principal quantum number, $L(i)$ is the total angular momentum quantum number, and $E(i)$ is the binding energy of the i^{th} excited state.

For the temperature of interest (3000 to 5000°K), cesium exhibits the largest average bound-free cross section through the solar spectrum. Cesium also has other important continuum absorption bands in the red portion of the solar spectrum as a result of cesium dimers. These absorption bands extend from about 6000 Å to 1 μm, which, conveniently, is where the bound-free cross section is falling off. The dimer absorption cross section may be computed from the quasi-static theory of line broadening.[9] This technique, which requires knowing the potential energy curves for the transition, partitions the molecular states into a set of substates characterized by their internuclear separation and populated relative to their dissociation products according to a classical conical ensemble. Thus, the concentration of dimers in the ground electronic state with an internuclear separation between R and R + dR is[10]

$$d[X] = 4\, R^2 dr (g_x/g_f) \exp(-WX(R)/kT)[Cs]^2 \quad , \qquad (3)$$

where [ ] indicate species concentration; g_x and g_f are the degeneracies of the molecular X state and its parent atomic state, respectively; $WX(R)$ is the energy of the molecular substate relative to that of its parent atomic state; k is Boltzmann's constant; and T is the gas temperature.

The absorption coefficient caused by a ground-state dimer transition can then be written as[9,10]

$$\beta_{Di} = \frac{\lambda^2}{2} \frac{AR^2}{d\nu/dR} \exp\,(-WX(R)/kT)(g_x/g_f)[Cs]^2 \quad , \qquad (4)$$

where A is the Einstein coefficient for the transition (assumed independent of R), and λ and ν are the wavelength and frequency of the radiation.

Rather than computing the dimer absorption by simply inputting the measured values of the dimer absorption cross section at an arbitrary temperature (as done, for example, in Ref. 11), we chose to compute the temperature-dependent absorption cross sections according to a four-Morse-potential state model of the cesium dimer molecule. Not only does this allow accounting for the temperature dependence of the cross section, it also assures that re-radiation is accounted for properly on the dimer transitions. The 8,000 to 10,000 Å X-A absorption band can be modeled fairly exactly in this way since it is due to transition to a single state. And although the shorter wavelength bands are actually caused by several overlapping transitions, the absorption can be modeled to an accuracy sufficient for our purposes by constructing three hypothetical Morse potential states with the parameters given in Table 1. Our computed absorption cross sections (shown in Figures 1 and 2) agree well with Weschler's measured values.[13] Line absorption is not included in the theoretical model since it contributes negligibly to the net energy flow in the plasma.

Table 1. Morse Potential Parameters for the Four-State Model of Cs_2 Absorption Spectra (X-state parameters from Ref. 12)

State	D, cm^{-1}	R_e, Å	W_e, cm^{-1}	Atomic State
X	3600	4.47	42	6S
A	5100	5.25	34	6P 1/2
B	1510	4.47	34.2	6P 1/2
C	500	5.7	15	6P 3/2

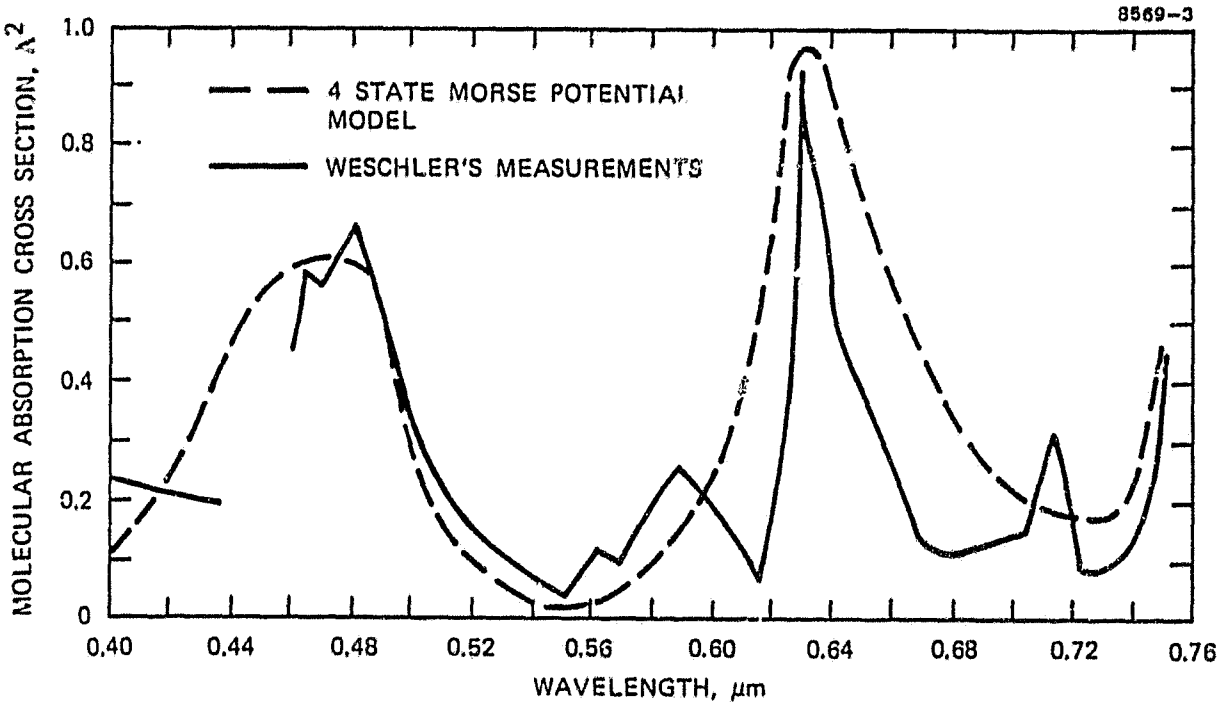

Figure 1. Computed and measured absorption cross sections of cesium vapor: 0.40 to 0.75 μm (measured values are from Ref. 13).

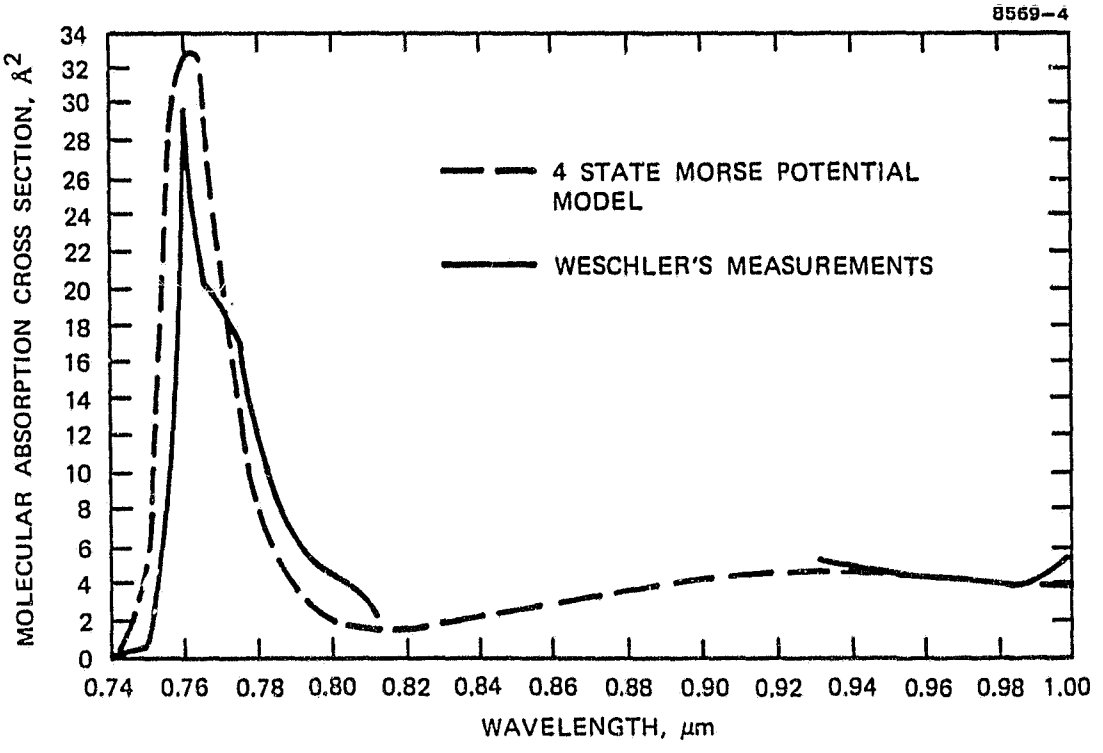

Figure 2. Computed and measured absorption cross sections of cesium vapor: 0.74 to 1.00 μm (measured values are from Ref. 13).

The net absorption coefficient due to both the bound-free transitions and the dimer transition illustrated in Figure 3 in an LTE cesium plasma at a temperature of 4000°K and a pressure of ∿2 atm is shown in Figure 4, where it is compared with the solar spectrum. Both the spectral profile and the magnitude of the cross section are shown to be well suited for the use of cesium at moderate densities as an efficient solar radiation receiver. These features and its relatively high vapor pressure at practical operating temperatures, its high electrical conductivity, and its availability identify cesium as an excellent working fluid for an advanced, high-temperature solar-electric heat engine.

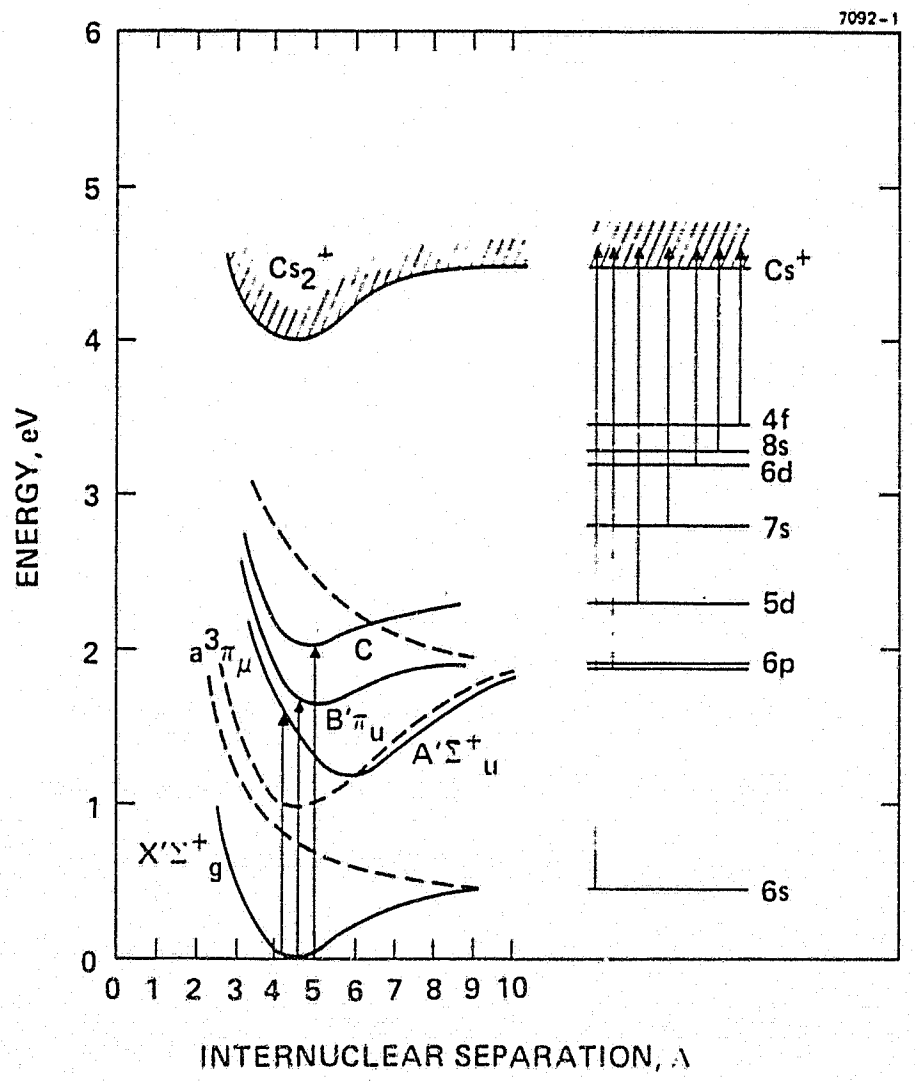

Figure 3. Cs and Cs_2 energy level diagram.

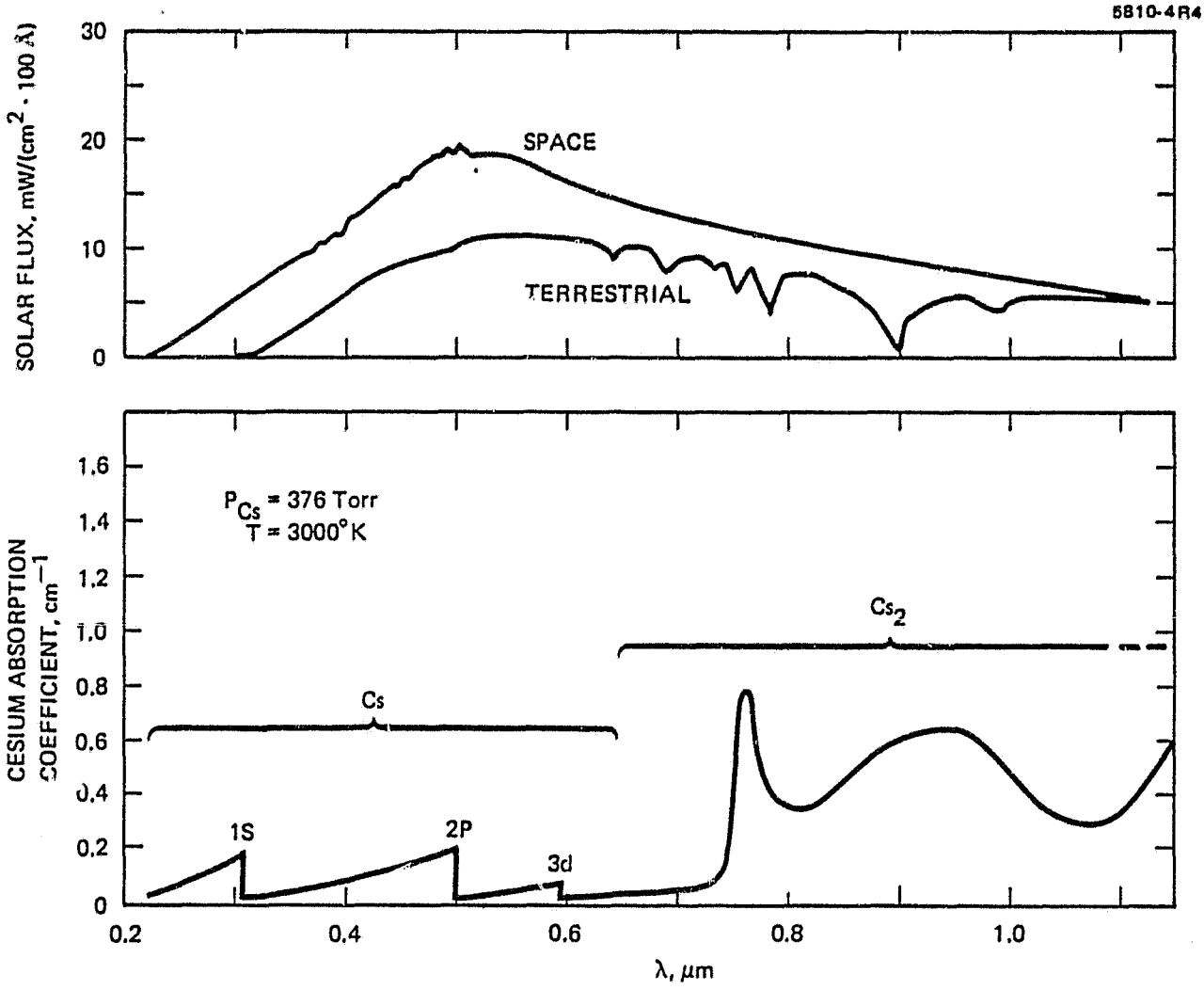

Figure 4. Solar spectrum and cesium absorption spectra.

B. IDENTIFICATION OF A HIGH-TEMPERATURE WORKING CYCLE

Having identified a cesium plasma as the optimal high-temperature collector for an advanced solar heat engine, our next task was to identify an optimal working cycle for converting the plasma thermal energy to electric power. The simplest and most direct way is to allow the plasma electrons themselves to carry the load current. There are only two mechanisms by which charge separation leading to net current flow out of the plasma can be accomplished in a thermal plasma:

- Charge separation caused by ambipolar diffusion (Weymouth plasma diode, TELEC-like devices)[14,15]
- Charge separation caused by $\vec{J}x\vec{B}$ forces (MHD).

In the first method, electric power coupled out of the plasma via ambipolar diffusion is essentially a surface rate that is independent of density and depends inversely on the smallest dimensional scale of the plasma:

$$P_{amb}\left(\frac{W}{cm^2}\right) \simeq \frac{fD_a\ (1.4 \cdot 10^{-23})\ T_e}{x} \quad , \tag{5}$$

where f is the degree of ionization of the plasma, D_a is the ambipolar diffusion coefficient per unit density in cm^{-1}/sec, T_e is the electron temperature in °K, and x is the small dimension of the plasma in cm.

We estimated that, at the temperatures of interest (∿3500°K), the cesium plasma would be losing energy to radiation at an effective surface rate of about 10% of the blackbody rate:

$$P_{rad}\left(\frac{W}{cm^2}\right) \simeq 0.1\ (5.7 \cdot 10^{-12})\ T^4 \quad . \tag{6}$$

At $T \simeq 3500°K$, D_a is on the order of $10^{20}\ cm^{-1}/sec$.[16] Thus, at 3500°K, for ambipolar diffusion to compete with radiation in efficiently coupling electrical power out of the plasma, we must have

$$\partial/\partial x \gtrsim 10^2 \text{ cm}^{-1} \quad . \tag{7}$$

Unfortunately, this condition is totally incompatible with efficient coupling of the sun's radiation into the plasma. Therefore, ambipolar diffusion cannot be anticipated to be an acceptable thermal-to-electric conversion mechanism when applied to a solar-sustained plasma. This leaves MHD as the apparent optimal working cycle.

In the MHD cycle, the plasma thermal energy is converted to translational energy by expansion of the plasma into a lower pressure region as in a turbine cycle but with the conversion of the plasma flow energy to electricity taking place by action of the $\vec{J}\times\vec{B}$ force on the plasma rather than by a turbine. In this way, power can be coupled out of the plasma at a rate that can be made to compete with the radiation losses from the plasma.

The most important plasma parameter for an MHD working fluid is its conductivity. The electrical conductivity of a 1 atm pressure cesium plasma in the temperature range from ∿1800 to 3000°K is on the order of 10^2 to 10^3 mho/m (see Figure 5).[17] At a magnetic field of ∿10 kG, plasma conductivities of this order will require MHD duct lengths of ∿1 m for significant extraction of electrical power from the plasma enthalpy (see Figure 6).[18]

The Hall parameter is the other important parameter for an MHD plasma (electron-cyclotron frequency times mean-free time). The Hall parameter for a 1 atm pressure solar-sustained cesium plasma at temperatures of ∿3000°K is much greater than 1 for an ∿10-kG field. This permits using a Faraday generator configuration, which does not require the use of segmented electrodes. Enthalpy extraction efficiencies of 15% have recently been demonstrated with this type of generator.[1]

The optimal thermodynamic MHD working cycle was identified to be a simple Rankine super-heat cycle. A conceptual description of the cycle is presented below.

Solar radiation is admitted through a sapphire window and brought to a focus in a region adjacent to a reservoir of metallic cesium. The proximity of the cesium reservoir to the focal region is chosen such

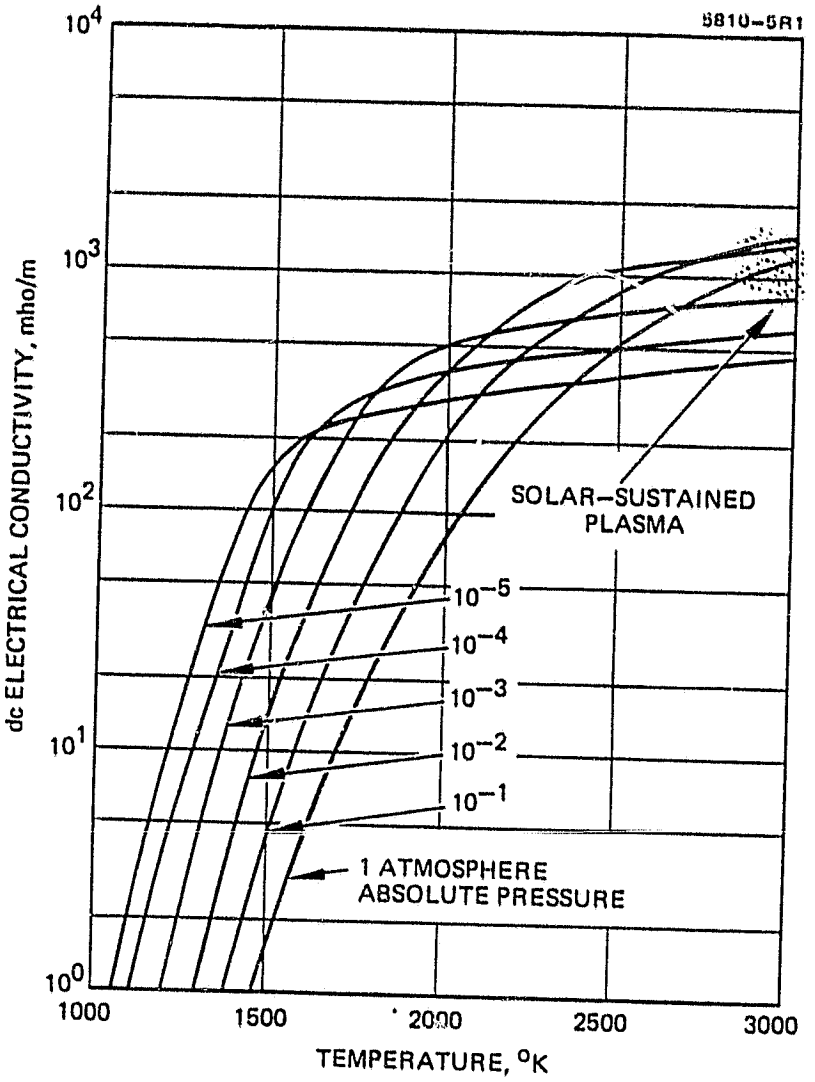

Figure 5. Electrical conductivity of a cesium plasma from Ref. 17.

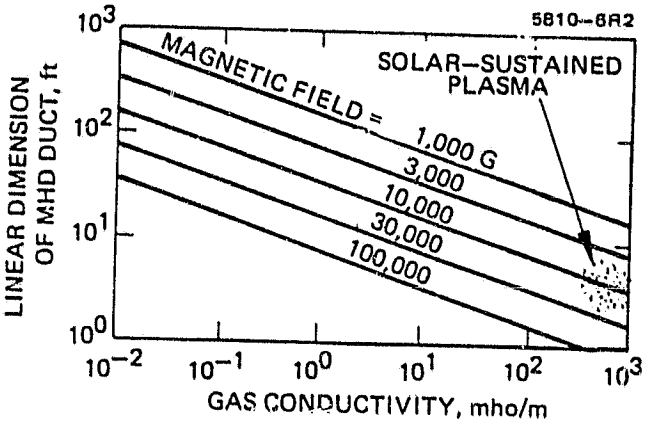

Figure 6. Required MHD duct length for conversion of plasma enthalpy to electric power from Ref. 18.

that radiation from the plasma will provide sufficient heating of the reservoir to give the desired vapor pressure. The sapphire window is placed far enough away from the focal region and cesium reservoir so that the condensation on the window can be prevented by local window heating.

Within the focal volume, the cesium vapor is brought to a temperature of about 3000°K by absorption on dimer transitions and excited state photoionizing transitions. The focal region forms the entrance to a plasma MHD duct. The duct is profiled so that the plasma will expand through it at a roughly constant velocity. The magnetic field strength within the duct is on the order of 10 kG which is provided by a superconducting magnet. It should be possible to control cesium condensation on the insulating walls of the duct by using either local heating or a buffer gas boundary layer.

After passing through the MHD duct, the cesium vapor is recondensed at a temperature of about 1000°K, corresponding to a pressure difference through the generator on the order of 1 atm. The molten cesium is then returned to the focal region reservoir by an electromagnetic liquid-metal pump.

A rough estimate of the scalability of the concept was obtained from the constraint that the aspect ratio of the MHD duct dimensions not exceed a value that would lead to excessive conduction losses. A previously used criterion would require that the ratio of the cross-sectional dimension to the length of the MHD duct not be less than $\sim 1/20$.[18] The minimum MHD duct length required for extraction of all of the plasma enthalpy is set by the stagnation pressure, the plasma conductivity, and the magnetic field. The stagnation pressure, of course, also determines the deposition length of the radiation in the plasma. Assuming a solar radiation concentration ratio of 10^3 (yielding a plasma temperature of $\sim$3000°K, which corresponds at 1 atm to a plasma conductivity of $\sim 10^3$ mho/m)[17] and assuming a 10-kG field, the minimum duct length appears to be $\sim$1 m,[18] corresponding to a minimum aperture of $\sim$10 cm or a minimum input power level of $\sim$10 kW.

C. RADIATIVE ENERGY BALANCE RESULTS

A theoretical radiation energy balance model was developed to investigate the limitations imposed by radiation losses alone in achieving high temperatures in a solar-sustained cesium plasma. The model was later expanded to include thermal conduction, convection, and gas flow, as would occur in the working fluid of a solar electric heat engine (see Section 2.D).

The basic assumptions of the model are that local thermodynamic equilibrium exists and that the electron and heavy particle temperatures are equal. Since, at the cesium vapor densities of interest ($\sim 10^{19}$ cm^{-3}), electron/heavy-particle collisional energy transfer rates will dominate radiative and other convective energy transfer rates, these assumptions will be vaoid; also, reabsorption of radiation is neglected.

In the static plasma model, the plasma temperature is assumed to be independent of position in the plasma. The temperature is computed by balancing the energy absorbed on the three dimer transitions and eight photo-ionization transitions of cesium against energy lost to spontaneous emission and radiative recombination into these same states. The radiative rates are calculated on the basis of detailed balancing applied to the absorption cross sections. Rates into and out of states higher than the eighth excited state of cesium were verified to contribute negligibly to the overall energy balance in the plasma.

The energy balance calculations were carried out with a computer program. The results are shown in Figure 7 as a plot of the required solar flux (in W/cm^2) for maintaining a cesium plasma against radiative losses versus the attainable plasma temperature. The solar spectrum was taken as the spectrum of a blackbody at a temperature of 5800°K. The concentration ratio required to achieve these fluxes for a 1 kW/m^2 solar flux assumed incident at the earth is shown on the right ordinate. The maintenance flux for a perfect blackbody is shown for comparison. For these results to be valid for the static plasma, the energy loss to thermal conduction must be small compared with the radiative losses, and the spatial extent of the plasma along the radiation propagation direction must be small compared with the smallest penetration depth of the

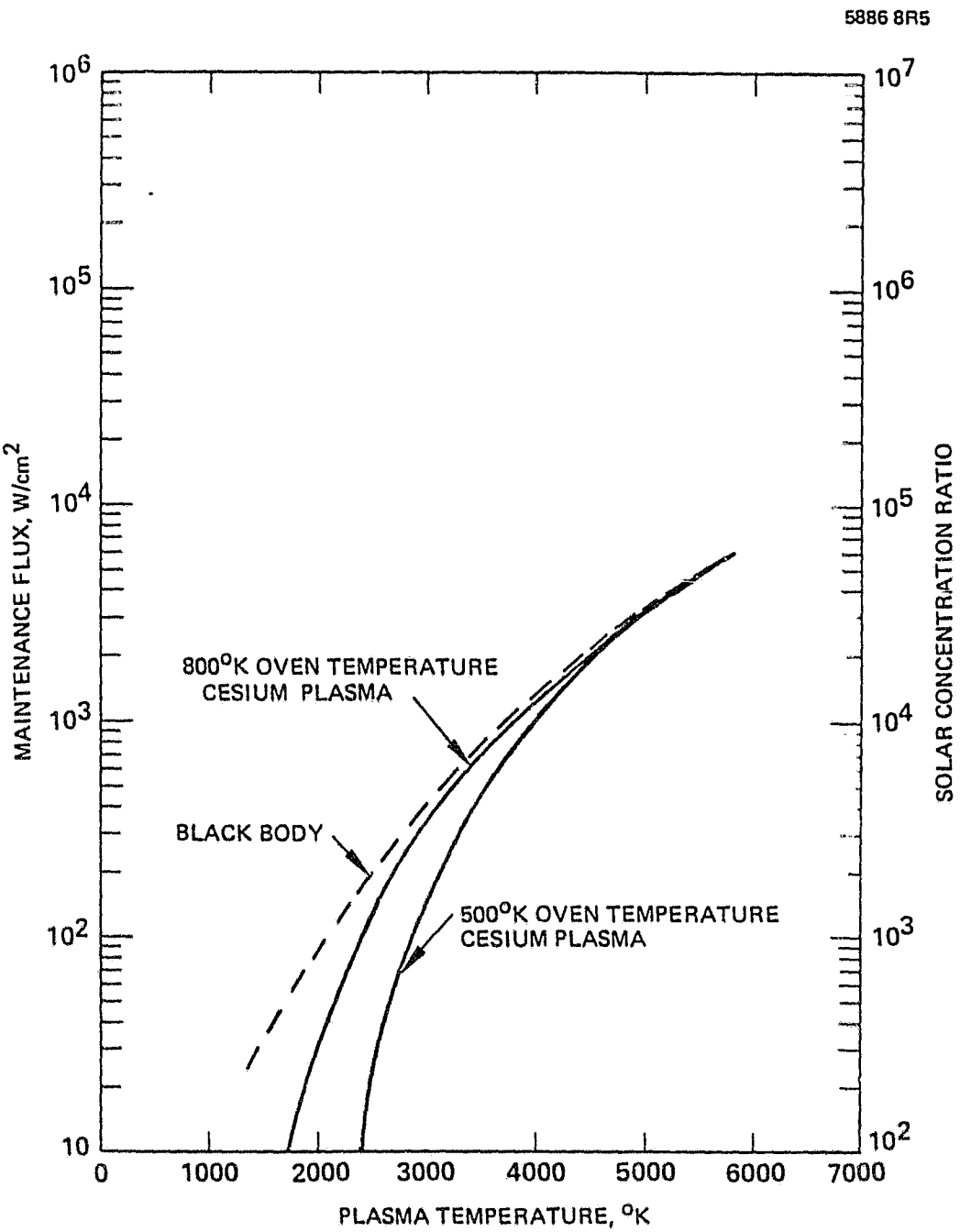

Figure 7. Radiation energy balance results.

solar spectrum in the plasma. These conditions will be approximately satisfied for a 1-cm-diameter spherical cesium plasma at the assumed density for the temperature range from ∿2500 to 4000°K. As shown in Figure 7, higher plasma temperatures result at lower oven temperatures in the purely radiative energy balance case because the lower fractional concentration of dimers causes the spectral range over which most of the absorption occurs to move to the shorter wavelengths associated with the bound-free transitions.

It is possible to understand the general form of the result presented in Figure 7 on the basis of a simple physical argument based on the principle of detailed balancing. The argument goes as follows.

Consider a system that is absorbing and emitting radiation on one transition only. If the system is in steady state, then the energy balance condition is

$$P(\nu)\sigma(n_\ell - n_u) = n_u A(h\nu) \quad , \tag{8}$$

where n_u and n_ℓ are the population densities of the upper and lower level for the transition, σ is the absorption cross section for the transition, A is the spontaneous radiative rate, and $P(\nu)$ is the input radiative power flux to the system at the transition wavelength. If the level populations are in thermal equilibrium at a temperature T, then, from detailed balancing, $P(\nu)$ is the Planck spectrum:

$$P_T(\nu) = \frac{2h\nu^3}{c^2} \left(e^{h\nu/kT} - 1\right)^{-1} \quad . \tag{9}$$

Alternatively, if blackbody radiation from a radiator of temperature T_R is to sustain the system at a temperature T, then the energy balance condition is

$$CP_{T_R}(\nu) = \frac{A}{\sigma}(\nu) \left.\frac{n_u}{n_\ell}\right|_T = P_T(\nu) \quad , \tag{10}$$

where C is a factor which is equal to one at the surface of the radiator. Obviously C = 1 for $T = T_R$. If $T_R \neq T$, then

$$C = \frac{P_T(\nu)}{P_{T_R}(\nu)} \quad . \tag{11}$$

From the form of the blackbody spectrum (Eq. 9), $C < 1$ for $T < T_R$ and $C > 1$ (optically impossible) for $T > T_R$. The above argument continues to hold (term by term) for a system absorbing blackbody radiation on more than one transition and, in particular, on the continuum bound-free and dimer transitions. The essential condition for the argument to be valid is that the system energy balance be dominated by radiation, that the input radiation be in a blackbody spectrum, and that the system be in thermal equilibrium at some temperature $T < T_R$.

In the case of several transitions or continuum transitions, the value for C will be determined from a spectrum integration of Eq. 11. In this case, one can write approximately:

$$C \simeq \left\{ \frac{\exp(h\bar{\nu}/T_R) - 1}{\exp(h\bar{\nu}/T) - 1} \right\} \quad , \tag{12}$$

where $\bar{\nu}$ is an average frequency of the absorption spectrum. This is the general form of the solid curves in Figure 7.

The re-radiation spectrum by the continuum absorption transitions is shown in Figure 8 for a selected plasma temperature. Although this radiation dominates line radiation in controlling the plasma temperature, line radiation will be a more useful signature of the plasma temperature due to its higher spectral brightness (see Section 3.C).

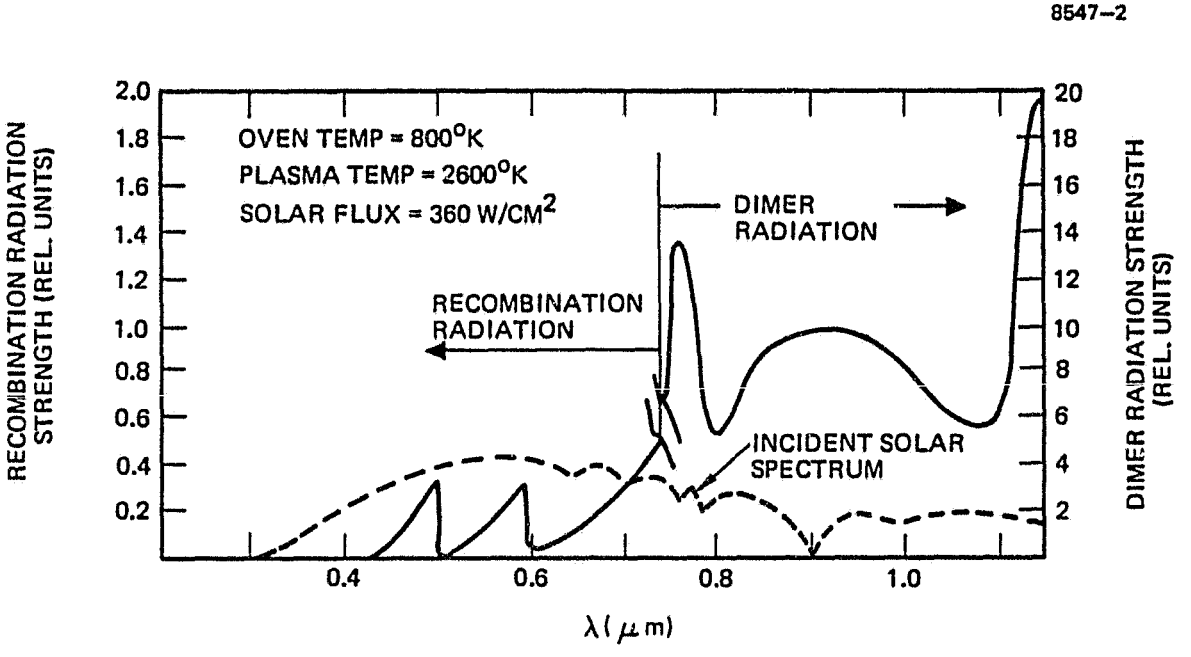

Figure 8. Theoretical continuum re-radiation spectrum (minus line emission).

D. TOTAL ENERGY BALANCE RESULTS

Lower oven temperatures result in reduced radiative energy deposition in the plasma, which will eventually make losses other than radiation dominate the energy loss from the plasma. Therefore, we have added both thermal conduction and free convection losses to the model. For the densities, convection velocities, and dimensional scales of the present experiments, the estimated Reynolds number for the plasma is quite small ($\sim$100), permitting the use of a kinematic value for the thermal conductivity coefficient for cesium vapor ($\sim 15.1 \cdot 10^{-5}$ W/cm°K).[19] Since the free convection flow was not viscosity limited for the dimensional scale of the present experiments, it was computed from buoyancy forces alone.[20] These nonradiative losses control the dependence of the plasma temperature on vapor pressure in our experiments for oven temperatures below about 800°K, as shown in Figure 9.

The model also accounts for the convergence of the incident radiation and computes the plasma temperature as a function of the propagation distance of the radiation into the vapor. The results, shown in Figure 10, show, for example, that higher plasma temperatures are attainable by positioning the focal volume as close as possible to the front boundary of the vapor.

Finally, for treating the flow of the plasma into a working cycle, we added a one-dimensional flow of the plasma along the propagation axis of the incident radiation to the model. The results are shown in Figure 11, in which it is assumed that the solar concentration ratio is 3000. Figure 11 shows the temperature, the fraction of incident radiation power remaining in the beam (transmitted power), and the fraction of incident radiation power contained in the plasma enthalpy flow (coupling efficiency). These are shown as functions of z for chosen values for the input flow velocity and ambient cesium vapor pressure.

The coupling efficiency equals one minus the sum of the fractional power transmitted and the fractional power radiated. The results show coupling efficiency to be maximum at the same downstream location as is temperature. In a heat-engine application, this location would be the optimal point at which to extract the cesium plasma working fluid from

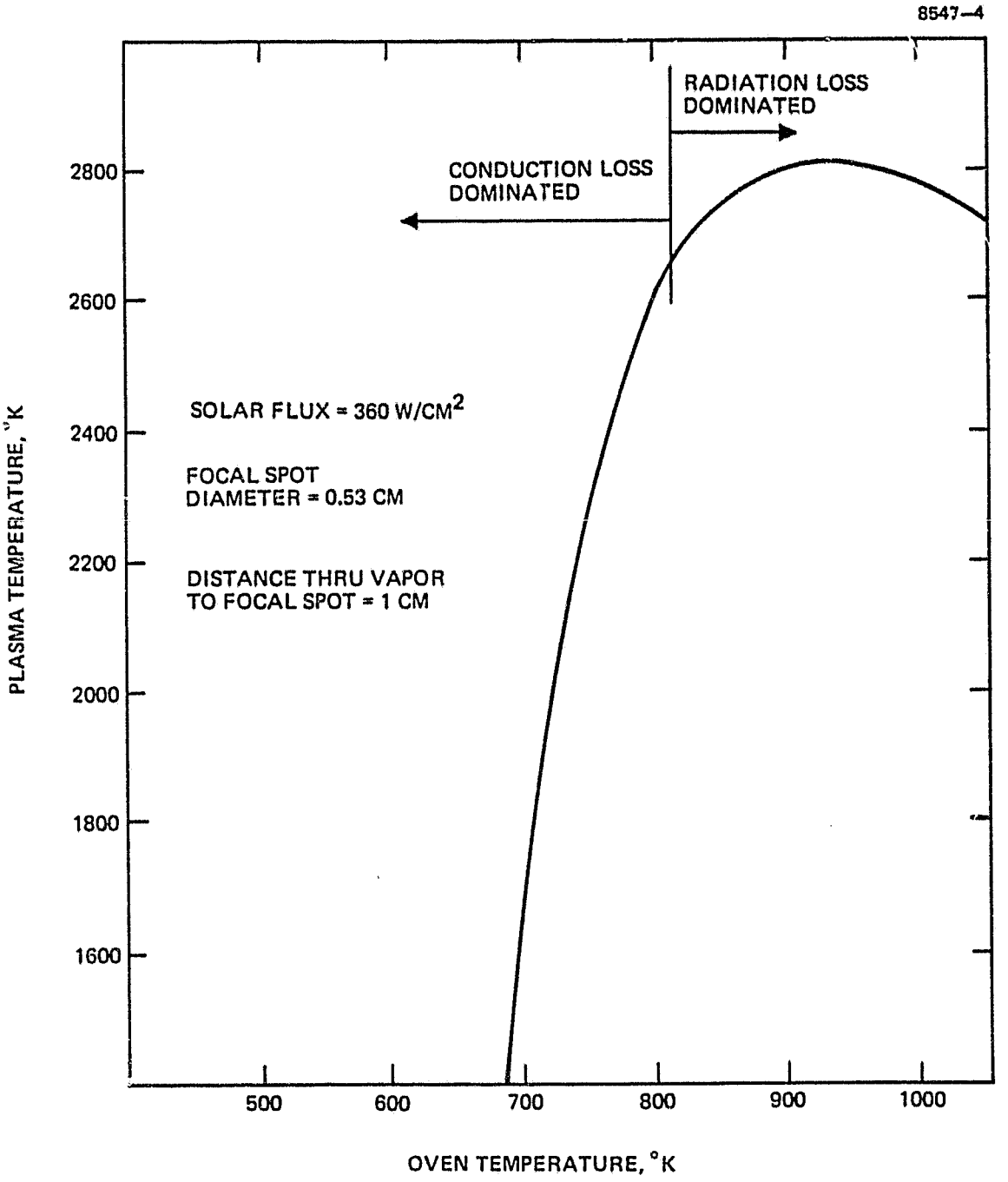

Figure 9. Theoretical plasma temperature as a function of oven temperature showing radiation- and conduction-loss-dominated regimes.

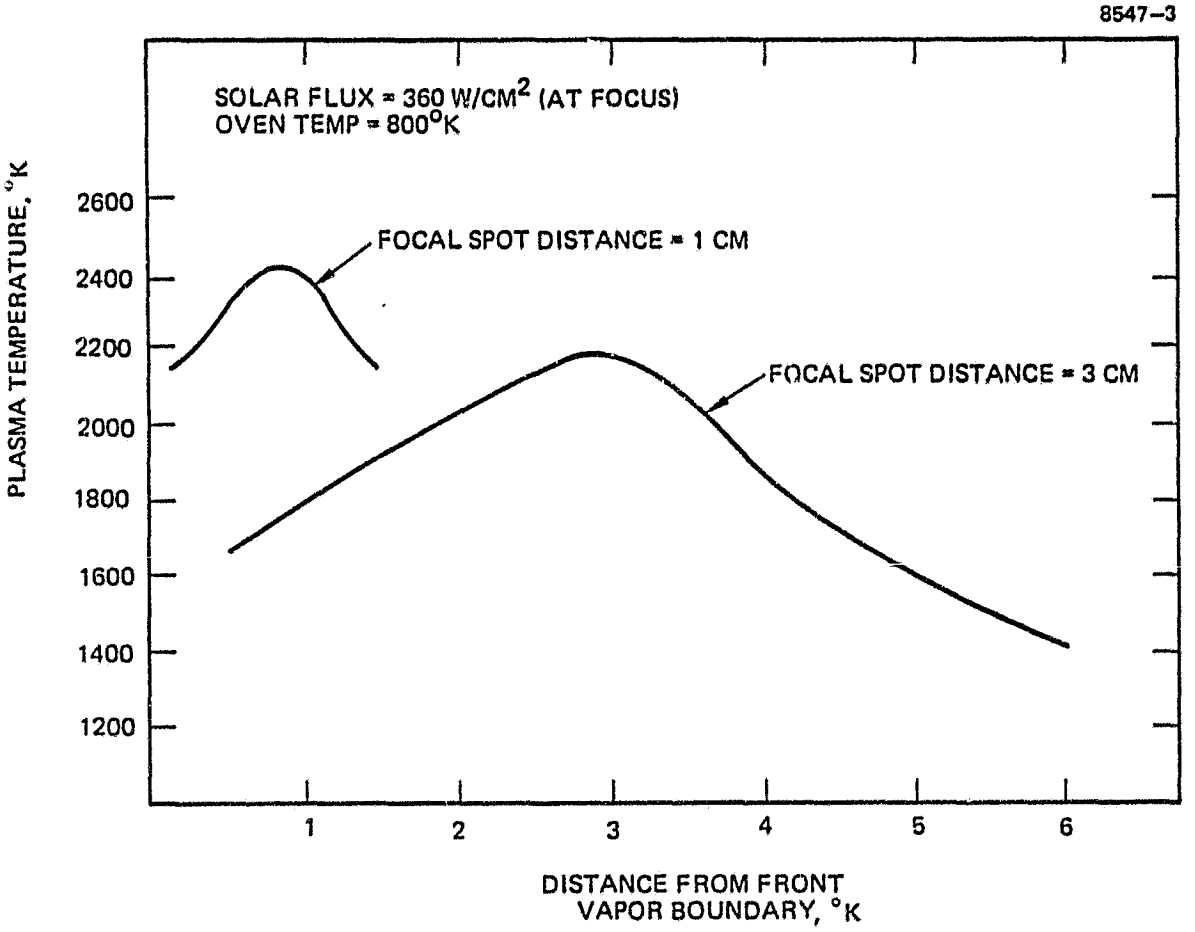

Figure 10. Plasma temperature as a function of distance from the front boundary of the vapor for two focal spot positions (theory).

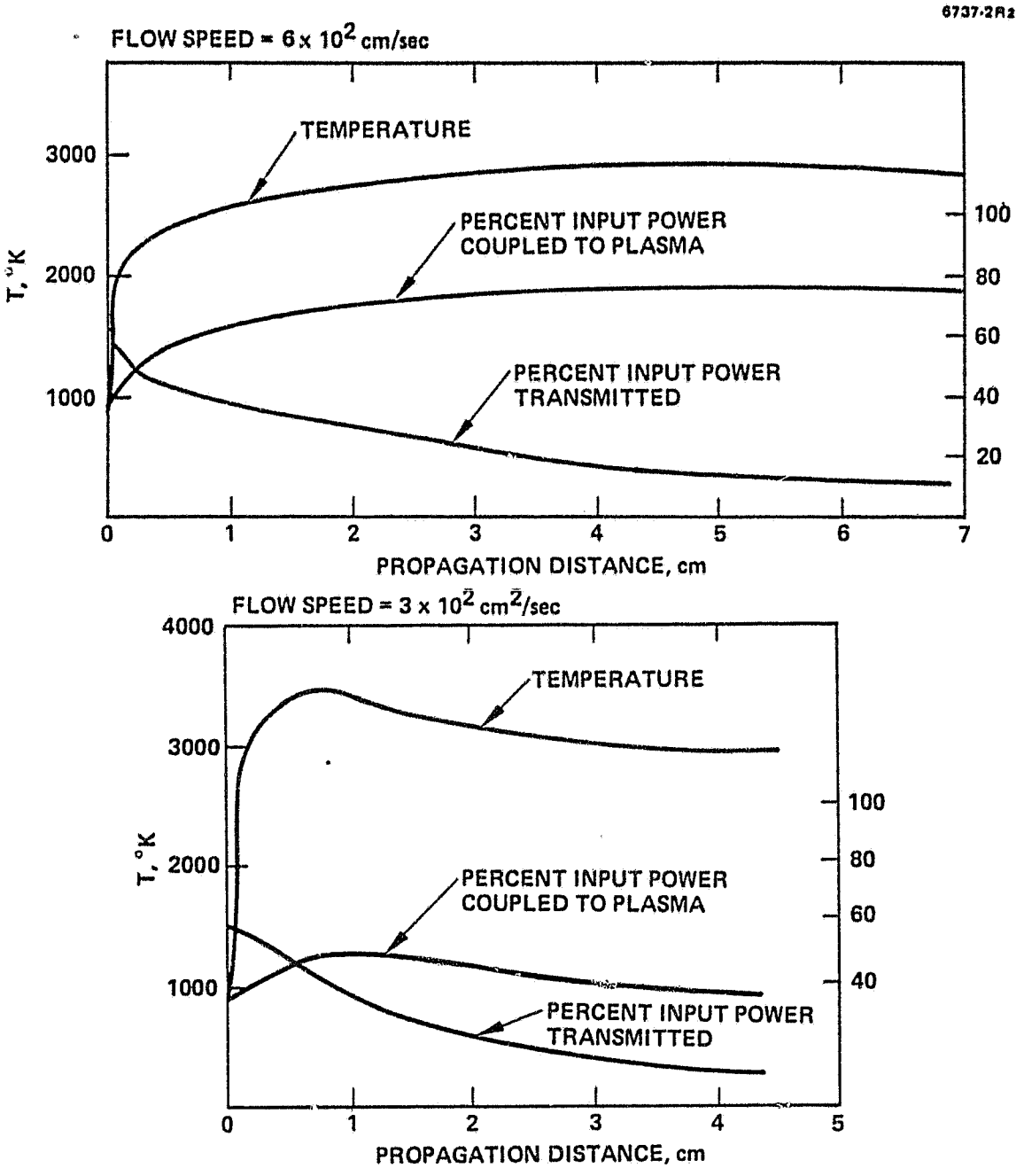

Figure 11. Plasma temperature, coupling efficiency, and transmission coefficient as a function of propagation distance in a cesium plasma from the one-dimensional convective model. (Oven temperature = 1000°C, solar concentration ratio = 3000.)

the radiation interaction zone. This interaction length scales proportionally with the flow speed and somewhat faster than inversely with the density (because of the influence of the dimer). There is a well-defined tradeoff between peak coupling efficiency and peak plasma temperature: higher flow velocities yield higher coupling efficiencies but (as expected) lower peak temperatures. Since, in a heat-engine application, the working cycle efficiency will generally increase with the input temperature of the working fluid, the requirement for maximum overall efficiency will determine an optimal flow speed through the radiation interaction zone.

All of the above plasma maintenance calculations are done with a computer program written for a PDP-10 computer. The flow chart for the computer program is presented in Appendix A.

E. SOLAR PUMPED LASER RESULTS

The concept of a solar-pumped MHD laser was first disclosed at the 1978 NASA Ames Conference on Radiation Energy Conversion and in the HRL technical proposal for this contract.[21] It was pointed out then that a population inversion on the cesium dimer A-X laser transition will develop in a solar-sustained cesium plasma if the electron temperature can be made to exceed the gas temperature by at least the fractional red shift of the transition. It was suggested that such a decoupling of the electron and gas temperatures could be made to occur in a nozzle flow of the plasma across a magnetic field. Thus, a closed Rankine cycle solar-pumped laser was identified that is similar in concept to the MHD solar-electric converter with laser power replacing or supplementing electric power as the work output of the cycle. The laser characteristics for this type of transition would include[10]

- High saturation power ($\sim$50 kW/cm^2)
- Large, high-power system capability (low gain, fewer parasitic problems)
- Broadband tunability ($\Delta\lambda \sim 1000$ Å).

During this program, we quantified these speculations with a mathematical model and expanded the lasing transitions considered to include the CsXe A-X excimer band. The excimer laser transition will offer essentially the same advantages as listed above for the dimer transition.[10] The results of the model appear favorable for the realization of laser action on the excimer transition in this system.

An energy level diagram showing the CsXe excimer and Cs_2 dimer laser transition is shown in Figure 12.[22] The fractional red shift is $\sim$0.07 for transitions from the bottom of the excimer A state and $\sim$0.23 for transitions from the bottom of the dimer A state. The two-temperature equilibrium model would predict a population inversion to occur on the excimer band for $T_e/T_g \gtrsim 14$ and on the dimer band for $T_e/T_g \lesssim 4.3$. These temperature ratios are easily attainable in a supersonic MHD flow (as will be seen below). However, for the plasma conditions we consider, several factors will conspire to invalidate the use of the simple two-temperature equilibrium model to determine the net gain on these laser transitions. These factors are discussed below.

The starting point for calculating the electron and gas temperature in a plasma flow through a short-circuited Faraday MHD channel is an electron energy balance equation derived by B. Zanderer et al.[23,24] and utilized in their program to generate 10-μm laser action in an MHD channel:

$$\frac{T_e}{T_g} - 1 = \frac{2}{3} M^2 \gamma \beta_e \delta^{-1} \quad , \tag{13}$$

where γ is the ratio of specific heats; β is the Hall parameter; M is the Mach number of the flow; and δ is an inelastic collision energy loss factor, which can be taken as equal to one plus the ratio of the inelastic electron collisional energy loss rate to the elastic collisional energy loss rate.[23,24] If a Maxwell-Boltzmann energy distribution is assumed for the electrons and the excited state populations of cesium, then δ may be estimated as[25]

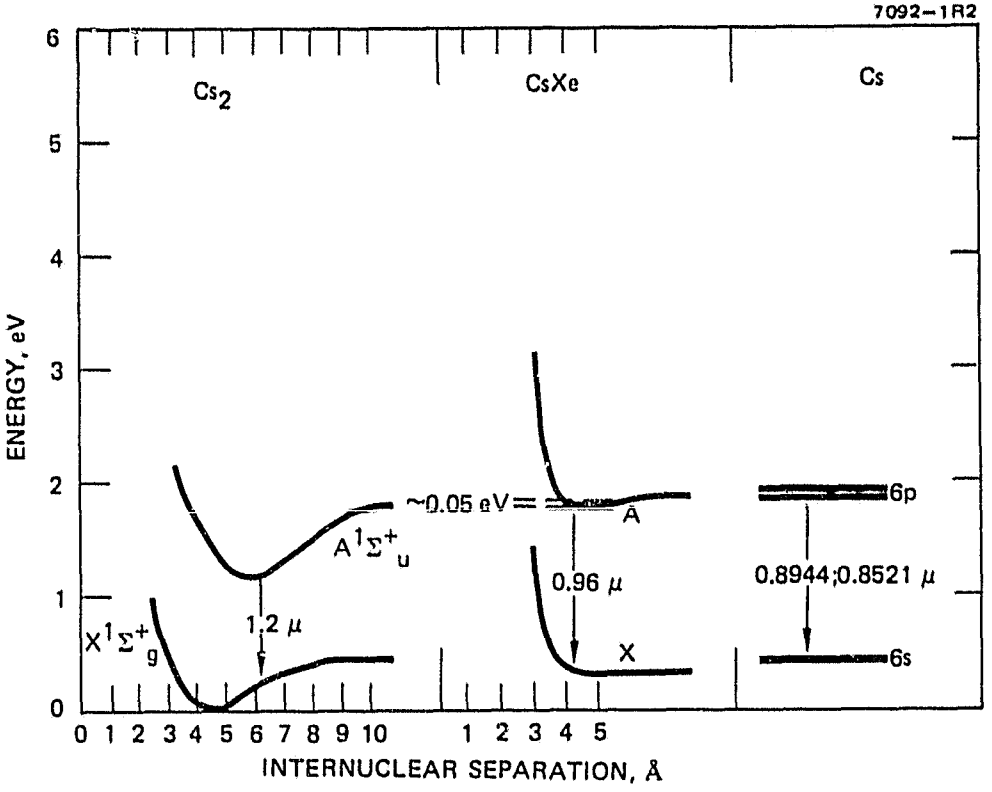

Figure 12. CsXe excimer and Cs_2 dimer laser transitions.

$$\delta = 1 + \frac{(6.38 \cdot 10^7)(2\,T_e)^{3/2}\,\exp(-E_1/T_e)(1 + E_1/2T_e)}{\sigma_{el}(2\,T_e/m_e)^{1/2}\,c(2m_e/m_{Xe})(T_e - T_g)} \left.\frac{d\sigma_1}{dE}\right|_{E_1} , \qquad (14)$$

where E_1 is the energy of the first excited state of xenon; σ_1 is its excitation cross section; σ_{el} is the electron elastic collision cross section; c is the speed of light; and the energies, temperatures, and masses are all expressed in eV.

If we add to Eqs. 13 and 14 the isentropic expansion equation for the gas temperature,[24]

$$T_g/T_o = \left\{1 + \frac{1}{2}(\gamma - 1)M^2\right\}^{-1} , \qquad (15)$$

where T_o is the stagnation temperature, then we may solve for the electron temperature and gas temperature as a function of the Mach number and the Hall parameter. We use $\gamma = 5/3$, $\sigma_{el} = 3 \cdot 10^{-15}$ cm^2, and $d\sigma_1/dE\big|_{E_1} = 3 \cdot 10^{-17}$ cm^2 eV^{-1}. The collision cross sections σ_{el} and $d\sigma_1/dE\big|_{E_1}$ were estimated from data on lithium in Ref. 26. The results for the electron temperature and the gas temperature are shown in Figure 13 as a function of Mach number for $\beta = 10$ and $T_o = 0.2$ eV.

The small-signal gain coefficients on the excimer and dimer bands can be computed from the quasi-static theory of line broadening:[10]

$$\text{gain} = \frac{\lambda^2\,\tau^{-1}}{8\pi}\left\{\frac{d[A]}{dR} - \frac{g_A}{g_X}\frac{d[X]}{dR}\right\}\frac{dR}{d\nu} , \qquad (16)$$

where λ and τ are, respectively, the wavelength and radiative lifetime of the transition; ν is the frequency of the transition at the internuclear separation R; [A] and [X] symbolize the concentration of the A and X states, respectively; and g_A and g_X are their degeneracies. The theory assumes that the molecular states are populated as a function of R according to a cononical ensemble so that we can write

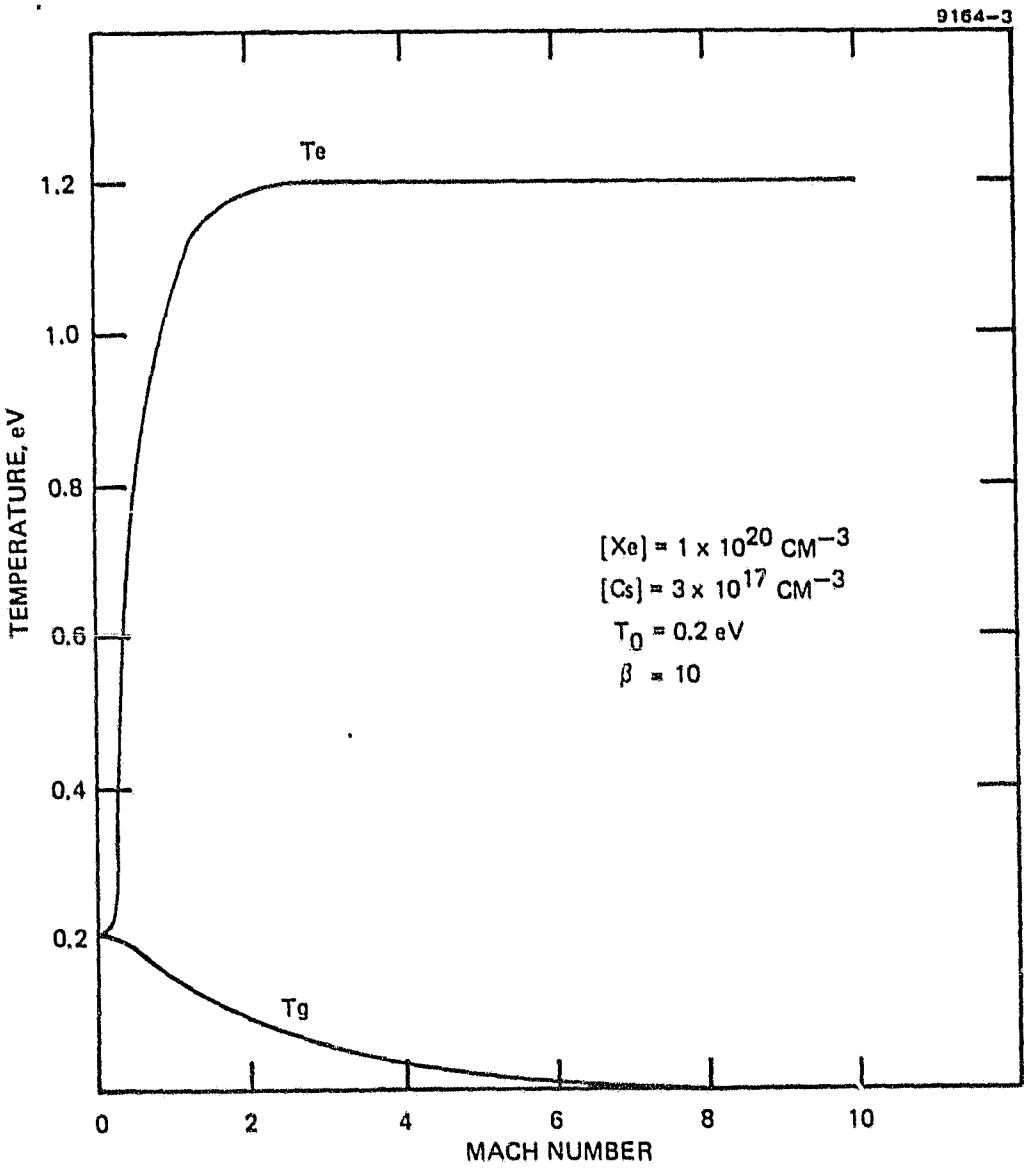

Figure 13. Electron and gas temperature as a function of Mach number for a cesium-xenon plasma flow in Faraday MHD channel.

$$\text{gain}(\lambda) = \alpha(\lambda) \left\{ \frac{[A]}{K_A} \frac{\exp(-V_A(\lambda)/kT_g)}{(g_{A,f}/g_A)} - \frac{g_A}{g_X} \frac{[X]}{K_X} \frac{\exp(-V_X(\lambda)/kT_g)}{(g_{X,f}/g_X)} \right\} , \quad (17)$$

where K_A and K_X are the A state and X state equilibrium constants, the $g_{,f}$s are the degenaracies of the atomic parent states, $V_A(\lambda)$ and $V_X(\lambda)$ are the potential energies of the A and X states at the internuclear separation corresponding to the transition wavelength λ, k is Boltzmann's constant, and $\alpha(\lambda)$ is the stimulated emission coefficient given by

$$\alpha(\lambda) = \left(\frac{1}{2\tau c}\right) R^2 \frac{dR}{d\nu} \quad . \quad (18)$$

At the temperatures and densities of interest here, the population of the CsXe A state is controlled by the heavy particle dissociation rate. In this case, both the A state population and the X state population will be in equilibrium with their parent atomic state, making the two-temperature equilibrium model for the population of the upper and lower molecular states of the excimer transition valid. However, in determining the net gain on the excimer level, one must also include the absorption on the X→A dimer transition since this absorption band overlaps the excimer gain band.[10] Under these conditions, we write the excimer gain as

$$\text{gain}_{ex}(\lambda) = \alpha_{ex}(\lambda) \left\{ [Cs^*][Xe] \frac{\exp(-V_A(\lambda)/kT_g)}{(g_{A,f}/g_A)} - \frac{g_A}{g_X} [Cs][Xe] \frac{\exp(-V_X(\lambda)/kT_g)}{(g_{X,f}/g_X)} \right\}_{ex}$$

$$- \alpha_{di}(\lambda) \left\{ \frac{[Cs_2]}{K_X} \frac{g_A}{g_X} \frac{\exp(-V_X/kT_g)}{(g_{X,f}/g_X)} \right\}_{di} , \quad (19)$$

where [Cs*] represents the concentration of cesium atoms in the 6P resonance state.

On the other hand, the Cs_2 A state population will not in general be in thermal equilibrium with the parent atomic state at the temperatures and densities of interest. The relatively large dissociation energy of this state will cause the collisional dissociation rate of the state to fall below its radiative rate at the lower temperatures and densities associated with high Mach numbers. With the radiative rate contributing to the net loss rate of the steady-state dimer A state population, Eq. 17 for the gain coefficient becomes

$$\text{gain}_{di}(\lambda) = \alpha_{di}(\lambda) \left\{ \frac{\Gamma_A\ [Cs^*][Cs][Xe]}{g_{A,f}/g_A} \frac{\exp(-V_A(\lambda)/kT_g)}{K_A(\tau^{-1} + \Gamma_A\ [Xe]/K_A)} \right.$$

$$\left. - \frac{g_A}{g_X} \frac{[Cs]^2}{g_{X,f}/g_X} \exp(-V_X(\lambda)/kT_g) \right\}_{di} , \qquad (20)$$

where Γ_A is the three-body association rate coefficient for the formation of the A state. The scaling arguments presented in Ref. 27 lead to an estimate of $\Gamma_A \simeq 1 \times 10^{-31} cm^6 sec^{-1}$ and $K_A \simeq 8 \times 10^{-23} \exp(-V_A/kT_g)$, where V_A is the potential energy at the bottom of the dimer A state well.

For the conditions we consider, the dissociation time of the dimer ground state will be comparable to the flow time of the plasma through centimeter-scale zones. Thus, the population of the dimer X state will not always be in equilibrium with the monomer concentration and in general will be given by

$$[Cs_2] = K_X\ [Cs]^2\ \{1 - \exp\ (\Gamma_{diss}\ [Xe]\ z/V_z)\} , \qquad (21)$$

where V_z and z are the flow velocity and distance along the flow, respectively, and Γ_{diss} is the dissociation rate constant for the X state and is related to the recombination rate constant and equilibrium constant by $\Gamma_{diss} = K_X\ \Gamma_X$. From Refs. 27 and 28, we estimate $\Gamma_X \simeq 1 \times 10^{-32} cm^{-6} sec^{-1}$. From Ref. 13 we find $K_X = 2.7 \times 10^{-23} \exp(-V_X/kT_g)$.

The maximum gain coefficient on the excimer and dimer bands occurs near 0.96 μm and 1.2 μm, respectively. Inserting in Eqs. 18 through 20 the R^2 and dR/dν values at these positions on the potential curves and the lifetime and relevant degeneracy factors from Ref. 10, we obtain

$$\text{gain}_{ex}(0.96\ \mu m) = 1.5 \cdot 10^{-37} \{\exp(0.05/T_g)\ \exp(-1.45/T_e) - \exp(-0.1/T_g)\}[Cs][Xe] - 2.0 \cdot 10^{-37} \{0.25/(2.7 \cdot 10^{-23})\}[Cs_2] \quad (22)$$

$$\text{gain}_{di}(1.2\ \mu m) = 2.0 \cdot 10^{-37} \left\{ \frac{0.25 \cdot 1 \cdot 10^{-31} \exp(-1.45/Te)}{(8 \cdot 10^{-23})\ 5.9 \cdot 10^{7} + 1 \cdot 10^{-31}\ [Xe]/(8 \cdot 10^{-23} \exp(0.63/Tg))} \right\} \cdot [Cs]^2\ [Xe] - 2.0 \cdot 10^{-37} \left\{ \frac{0.25}{(2.7 \cdot 10^{-23})} \right\} [Cs_2] \quad . \quad (23)$$

We have assumed that the population of the 6P resonance level at 1.45 eV is in equilibrium with the monomer ground state at the electron temperature. All temperatures are in eV, concentrations are in cm^{-3}, and the gain coefficients are in cm^{-1}.

The stagnation cesium density for the plasma flow was chosen to be compatible with the coupling of solar radiation to the plasma through dimensional scales on the order of several centimeters, while the xenon density was chosen to maximize the excimer gain for minimum magnetic field and Mach number. The chosen stagnation densities were:

$$[Cs]_o = 3 \cdot 10^{17}\ cm^{-3} \quad (24)$$

$$[Xe]_o = 1 \cdot 10^{20}\ cm^{-3} \quad . \quad (25)$$

At an assumed temperature of 0.2 eV for the solar-heated plasma, these densities correspond to a stagnation pressure of ∿20 atm.

Figure 14 shows the results for the small-signal gain coefficients on the dimer and excimer bands computed for these conditions as a function of Mach number using Eqs. 13 through 23. The figure also shows the approximate magnetic field required to maintain the assumed value of 10 for the Hall parameter. These results show that positive gain coefficients are available on the excimer band near a Mach-2 flow and above about a Mach-7 flow. The dimer gain remains negative throughout the entire range.[29] The minimum gain region around Mach 4 roughly divides the kinetic regime for the ground state dimers into a regime where the dimers are in equilibrium with the monomers for smaller Mach numbers and a nonequilibrium regime for larger Mach numbers. This is illustrated further in Figure 15. The Mach-2 excimer gain is shown to be constant with distance in the flow, indicating that equilibrium concentrations of all species involved in determining the excimer gain have been reached. On the other hand, the Mach-7 excimer gain is seen to fall linearly with distance, which reflects the increasing concentration of absorbing ground state dimers with distance as they approach their equilibrium values at some distance much further down stream.

The high-Mach-number regime for positive excimer gain extends over a broader range of flow parameters and does not require the high magnetic fields that the low-Mach-number regime does. Also, it represents a kinetics regime for the alkali rare gas excimer laser that has not yet been explored experimentally.[30] Thus, if these high Mach numbers can be attained in this type of plasma, this regime would appear to offer the greatest potential for the first demonstration of an alkali rare gas excimer laser.

Arc or chemical heating might be used as an alternative to solar heating the plasma. Shock tube experiments utilizing an arc-heated plasma probably represent the most expedient means for performing the initial experimental investigations of the concept.

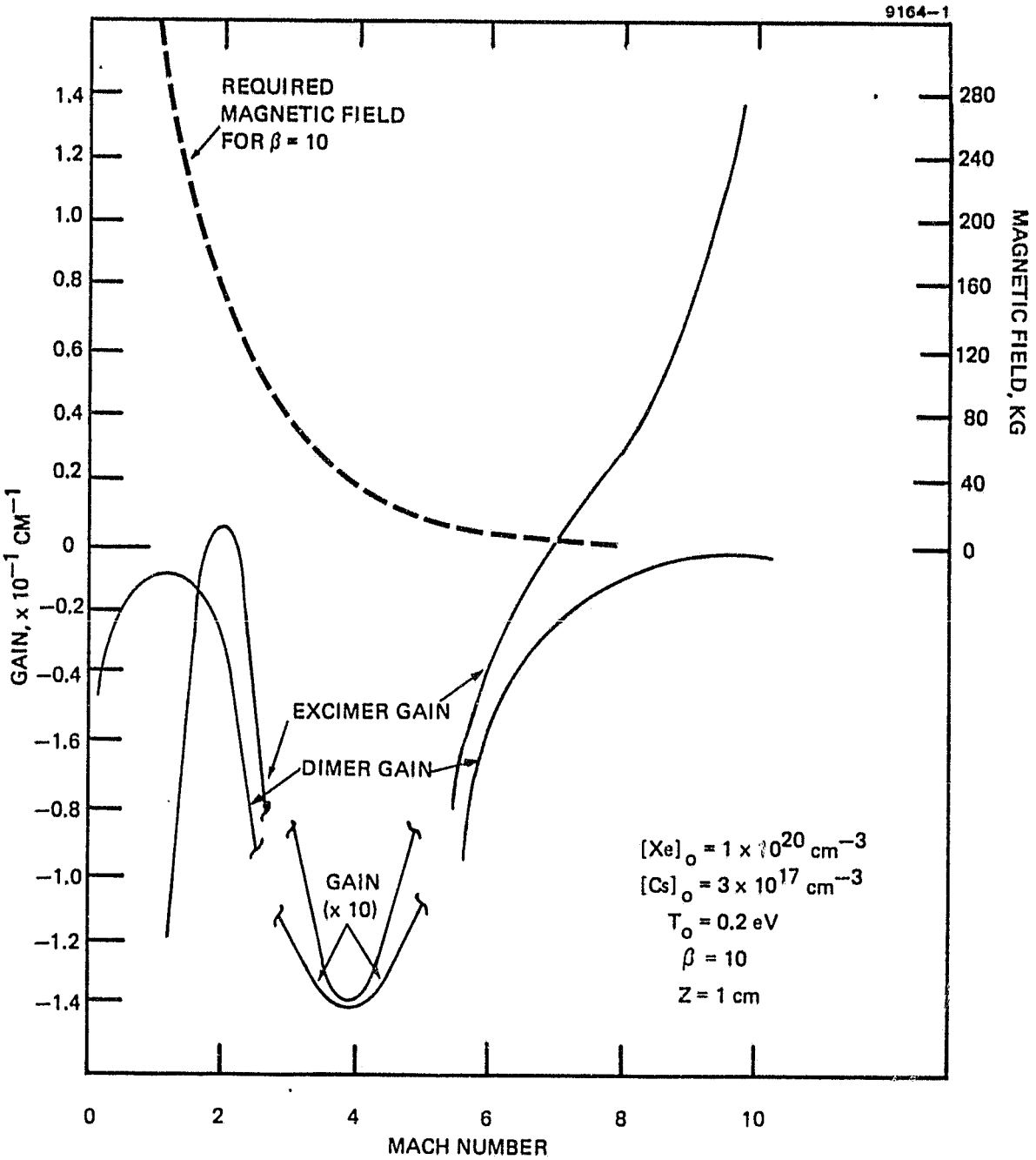

Figure 14. Small signal gain coefficients and required magnetic field versus Mach number for a cesium-xenon plasma in a Faraday MHD channel.

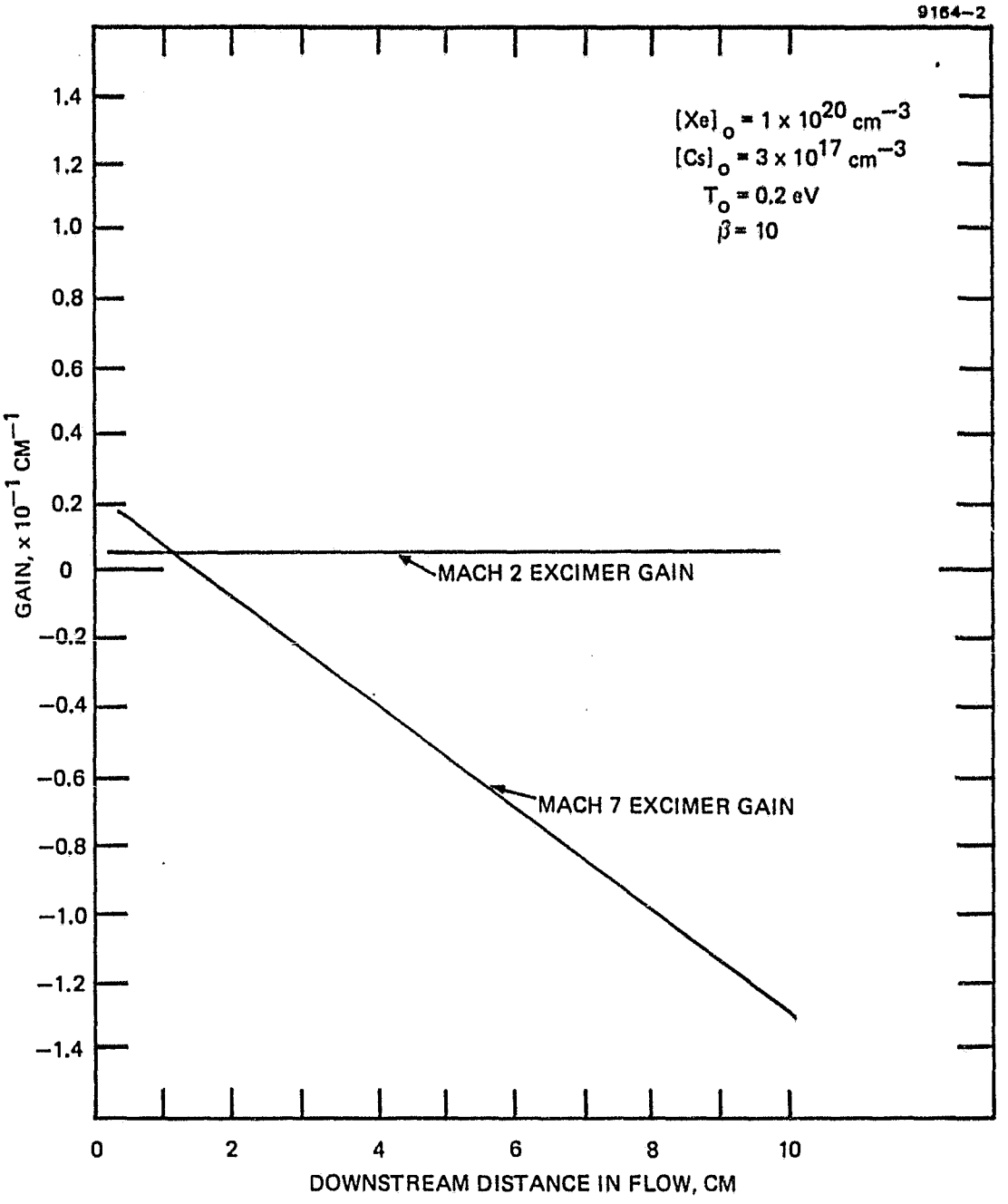

Figure 15. Small signal excimer gain coefficient versus downstream distance for a cesium-xenon plasma in a Faraday MHD channel.

SECTION 3

EXPERIMENTAL PROGRAM

A. RADIATION SOURCES

Two alternative radiation sources were used on this program. A 15-in. Fresnel lens solar concentrator mounted on an equatorial tracking mount was made available for outdoors use. The equatorial mount was large enough to accommodate both the cesium absorption cell and a 1/4-m Jarrel ash monochromator and vidicon tube assembly. This apparatus is shown in Figures 16 and 17. The parameters of the Fresnel lens concentrator are presented in Table 2.

For indoor use, a 1600-W xenon arc lamp adapted with a 10-in.-diameter elliptical reflector for simulating concentrated sunlight was purchased by HR as capital equipment for use on this program. This solar simulator is shown in Figure 18. The radiation flux profile provided at the focal plane of this source is shown in Figure 19. The peak radiation flux of $\sim$30 W/cm^2 is equivalent to a solar concentration ratio of about 300.

Table 2. Parameters of Solar Concentrator

LENS DIAMETER	38 cm (15 in.)
FOCAL LENGTH	61 cm (24 in.)
f	1.6
AREA	1140 cm^2
TRANSMISSION	85%
SOLAR IMAGE DIAMETER AT FOCAL PLANE	tan 0.5° x 61 cm = 0.53 cm
SOLAR IMAGE AREA AT FOCAL PLANE	0.222 cm^2
MAXIMUM CONCENTRATION RATIO AT FOCAL PLANE	$\frac{1140}{0.222} \cdot 0.85 = 4365$
MAXIMUM COLLECTED POWER DENSITY AT FOCAL PLANE (AIR MASS ONE 86.5 mW/cm^2)	$4365 \cdot 86.5 \cdot 10^{-3} = 377$ W/cm^2
POWER COLLECTED FOR 1 cm^2 ROUND CELL (DEFOCUSSED)	$1140 \cdot 86.5 \cdot 10^{-3} \cdot 0.85 = 84$ W
POWER COLLECTED FOR 1 cm^2 SQUARE CELL (DEFOCUSSED AND MASKED)	$84 \text{ W} \cdot \frac{\pi}{8} = 33$ W
POWER DENSITY CONCENTRATION RATIOS	1 cm^2 ROUND CELL $1140 \cdot 0.85 = 969$
	1 cm^2 SQUARE CELL $969 \cdot \frac{2}{\pi} = 617$

M12788

Figure 16. Experimental set-up utilizing solar concentrator heliostat.

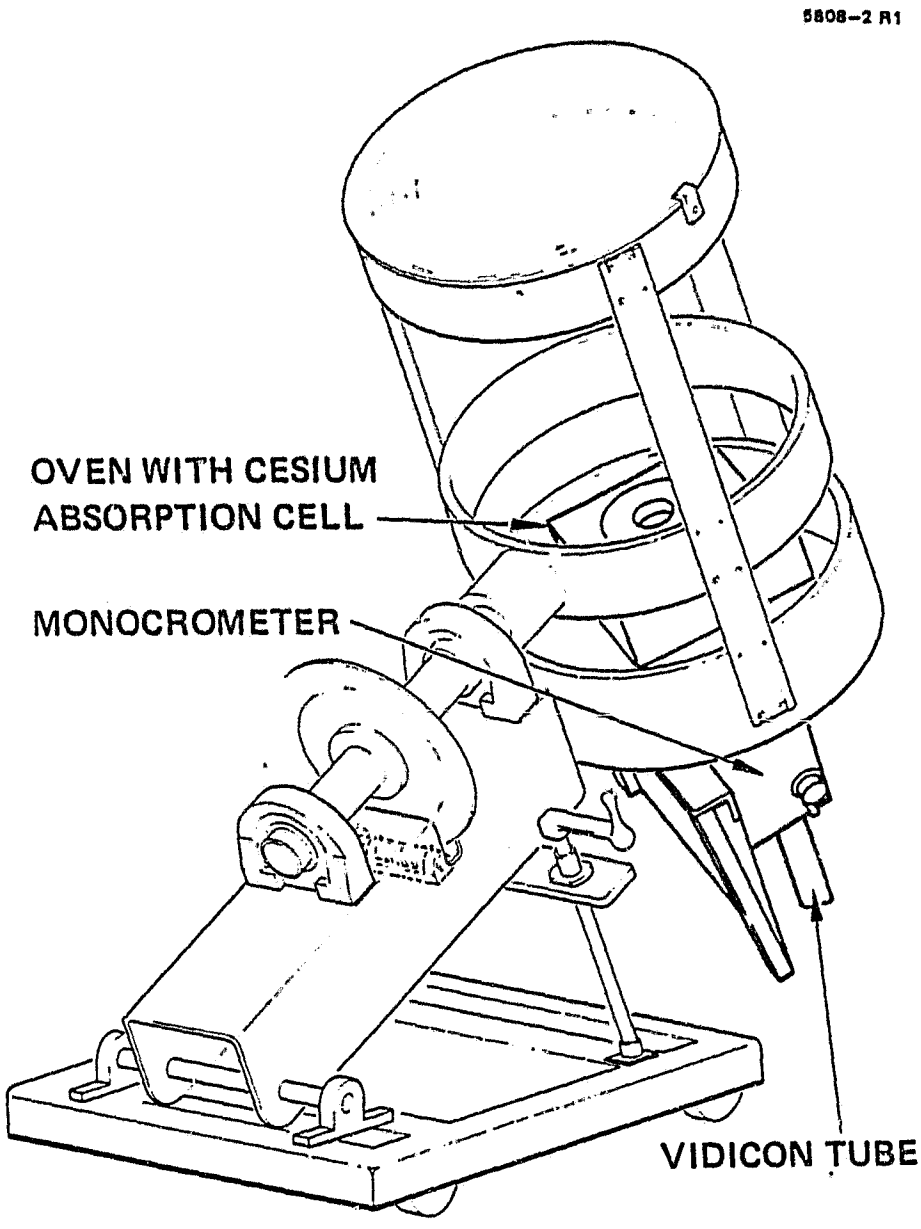

Figure 17. Heliostat-concentrator apparatus.

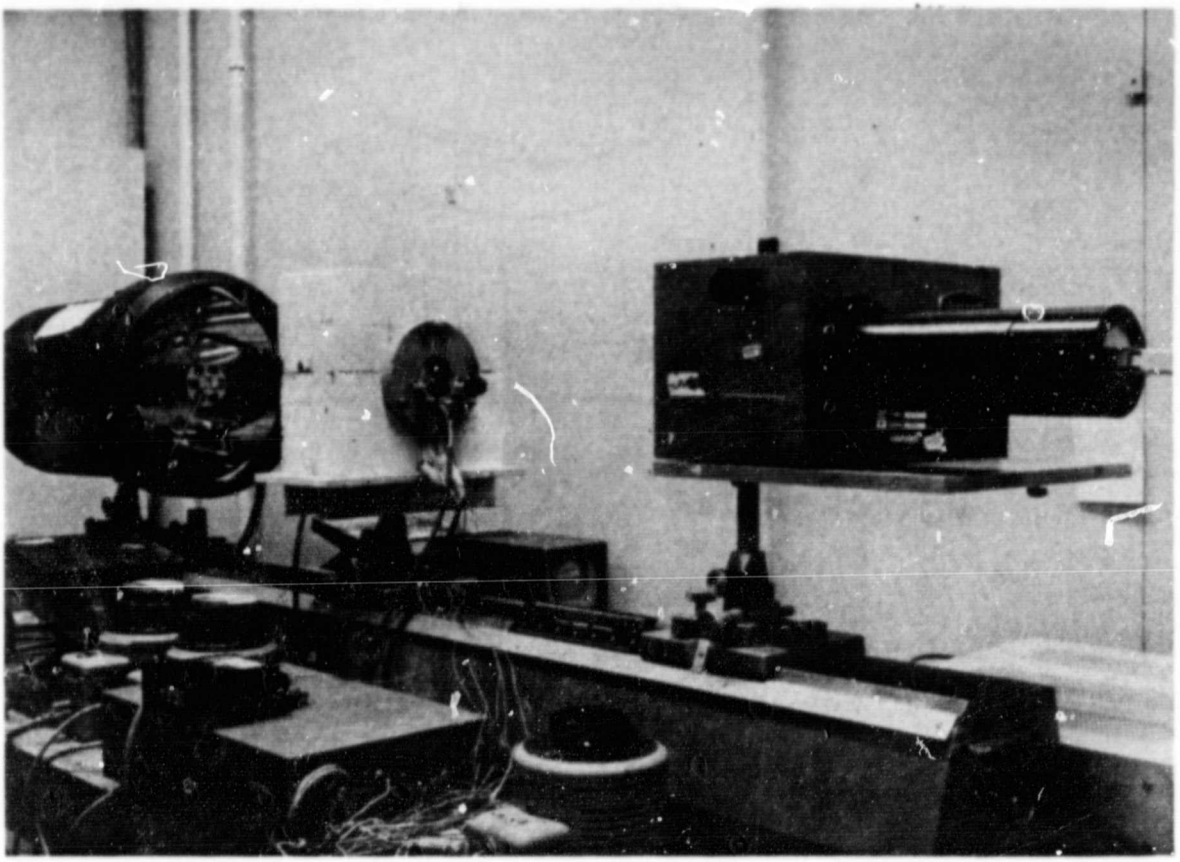

Figure 18. Experimental set-up utilizing arc lamp solar simulator.

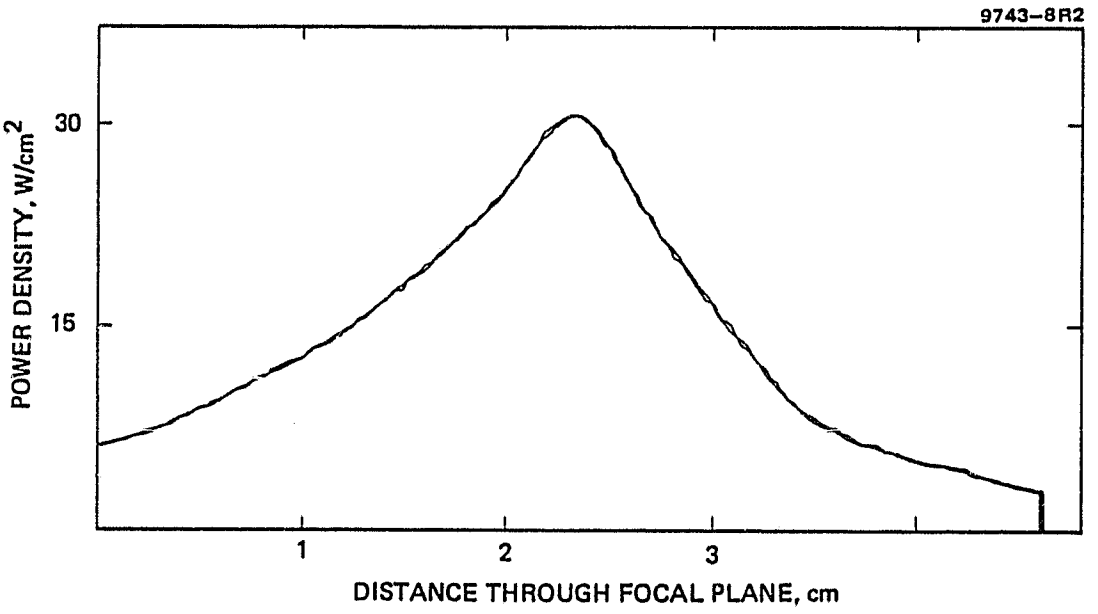

Figure 19. Solar simulator focal volume irradiance profile.

B. CESIUM VAPOR CELLS

The first design selected for the cesium absorption cell is shown in Figure 20. This cell was fabricated by ILC Corporation (Sunnyvale, California). It has two 1-in.-diameter sapphire windows (brazed to the cell with an alkali-resistant braze and an internal depleted uranium getter. ILC vacuum baked the cell, loaded it with cesium, and sealed it. They specified the cell to be capable of operating to at least 650°C.

The main problem with this cell was window fogging, which continued to occur with this cell design even when high-power window heaters were used. Also, the entrance window on the cell cracked twice when the solar simulator was used with it, as shown in Figure 21, causing a long delay during repair of the cell at ILC Corporation. This cell design ultimately had to be abandoned because of these window failures, but a series of experiments were carried out with the cell in the solar concentrator; these are described in Section 3.C.

We now feel that window fogging in this cell could probably be reduced substantially by using an appendage in the cell that is kept colder than the cell body, thus serving as a reservoir for liquid cesium. Also, since the entrance window broke only when the solar simulator was used, we suspect the cause to be the absorption in the sapphire of far-IR radiation from the arc lamp. This could be eliminated by using an IR blocking filter.

After the second window failure, we decided to convert the absorption cell design to that of a heat pipe oven. Heat pipe ovens offer several advantages over equilibrium ovens, such as uniform temperature vapor zones, vapor purification, and isolation of the vapor from the windows.[31] The latter feature is especially important for our application because it allows using ordinary glass windows and should eliminate the window fogging problem by separating the cesium vapor zone from the zone adjacent to the windows. Since the vapor pressure in a heat pipe oven is determined by the pressure of the inert gas in the oven,[31] the cell design included a valve to permit changing the vapor pressure and moving the cell outside when the solar concentrator is used.

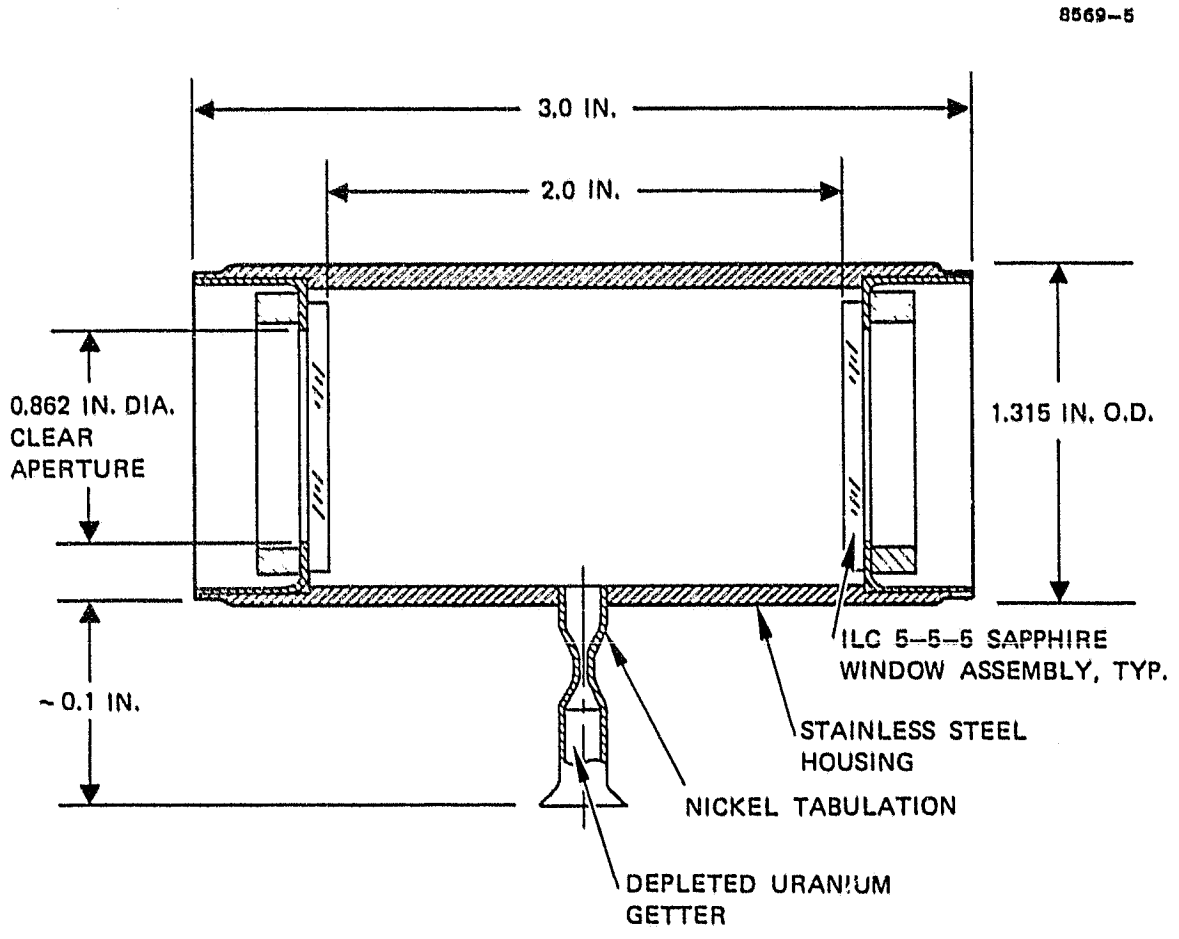

NOTES:

1. DEVICE VACUUM BAKED AT 600°C
2. FILLED WITH 10 mg CESIUM

Figure 20. Original ILC Corp. cesium cell design.

M12908

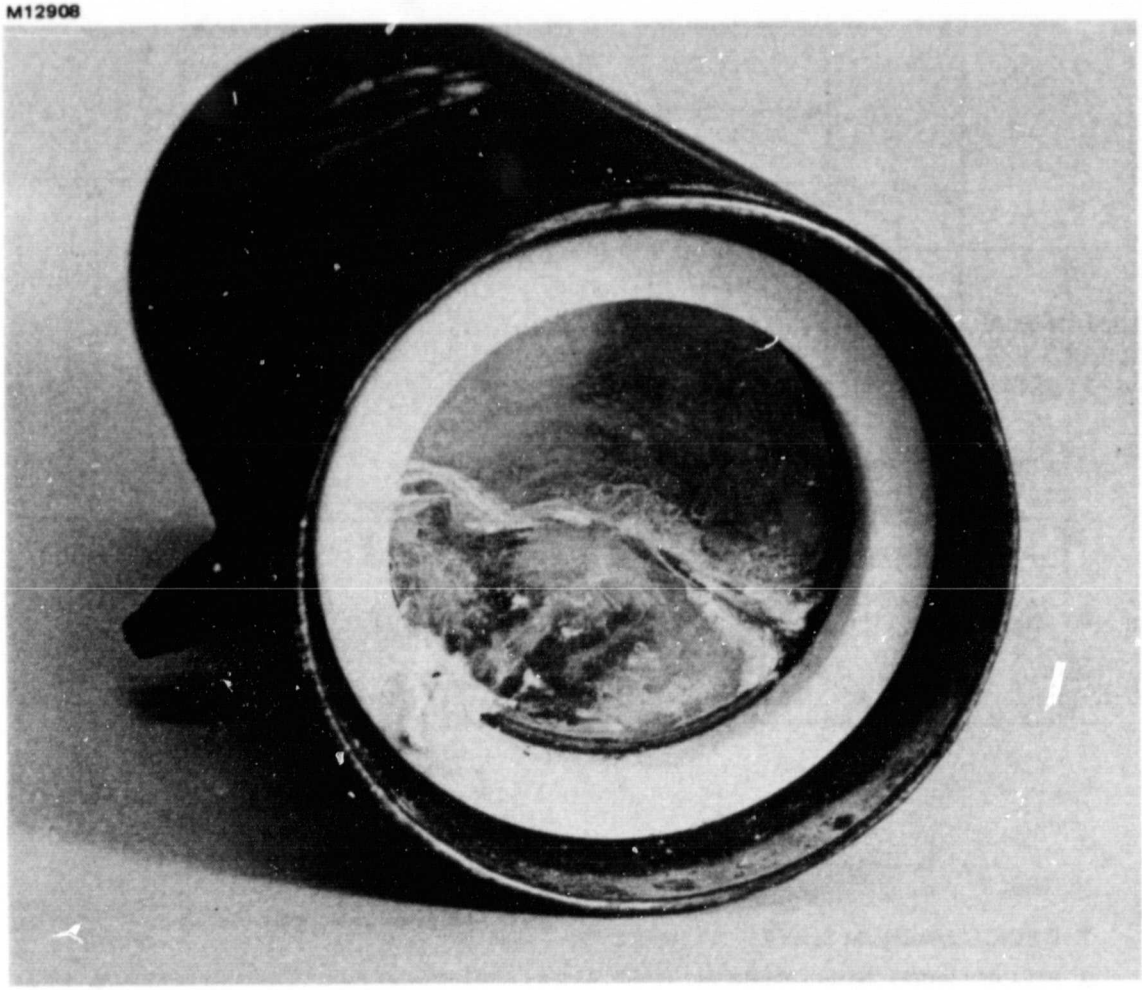

Figure 21. Cracked entrance window of ILC cell.

The design of the heat pipe oven underwent three major changes during the experiments. This design evolution, shown in Figure 22(a, b, and c), was an effort to eliminate window fogging in the low-aspect-ratio cell geometry required to interface converging radiation with the cell. Window fogging was finally reduced to a tolerable level by using the conical baffles illustrated in Figure 22(c). These baffles allow the incident radiation to pass into the central region of the cell relatively unobstructed while reducing the size of the convection cells in the end region of the cell to a small enough scale so that the cesium is deposited on the baffles rather than on the window. Operating the cell in a vertical configuration (with the lower end of the central zone sealed off) reduced the window fogging further and allowed the cesium deposited on the baffles to drain back into the central region.

The cesium vapor pressure could be maintained at temperatures between 500 and 600°C for indefinite periods. The window does not fog as long as the illumination time by the solar simulator is kept to a period of ∿1 to 2 sec at a time. The focal volume region in the vapor is viewed with an optical multichannel analyzer through the entrance window using a carefully aligned, shielded optical train. A photograph of the cell in the experimental setup in which the final demonstration of plasma heating was achieved is shown in Figure 23.

The final piece of experimental apparatus fabricated on this program was a heat pipe cell with transverse viewing ports and precision-made conical baffles. This cell is shown in Figures 24 and 25. Funding limitations prevented carrying out any experiments with this cell.

C. EXPERIMENTAL RESULTS

The first experimental indications of plasma formation by solar heating were obtained with the equilibrium cesium cell used with the Fresnel lens solar concentrator, as shown in Figure 16. The cell was operated at ∿500°C, and the cesium dimer absorption bands near 4500 Å and 5200 Å were monitored as the intensity of the incident focused sunlight was brought from an attenuated level to full illuminance. The results are shown in Figure 26. The reduced absorption gradients as a

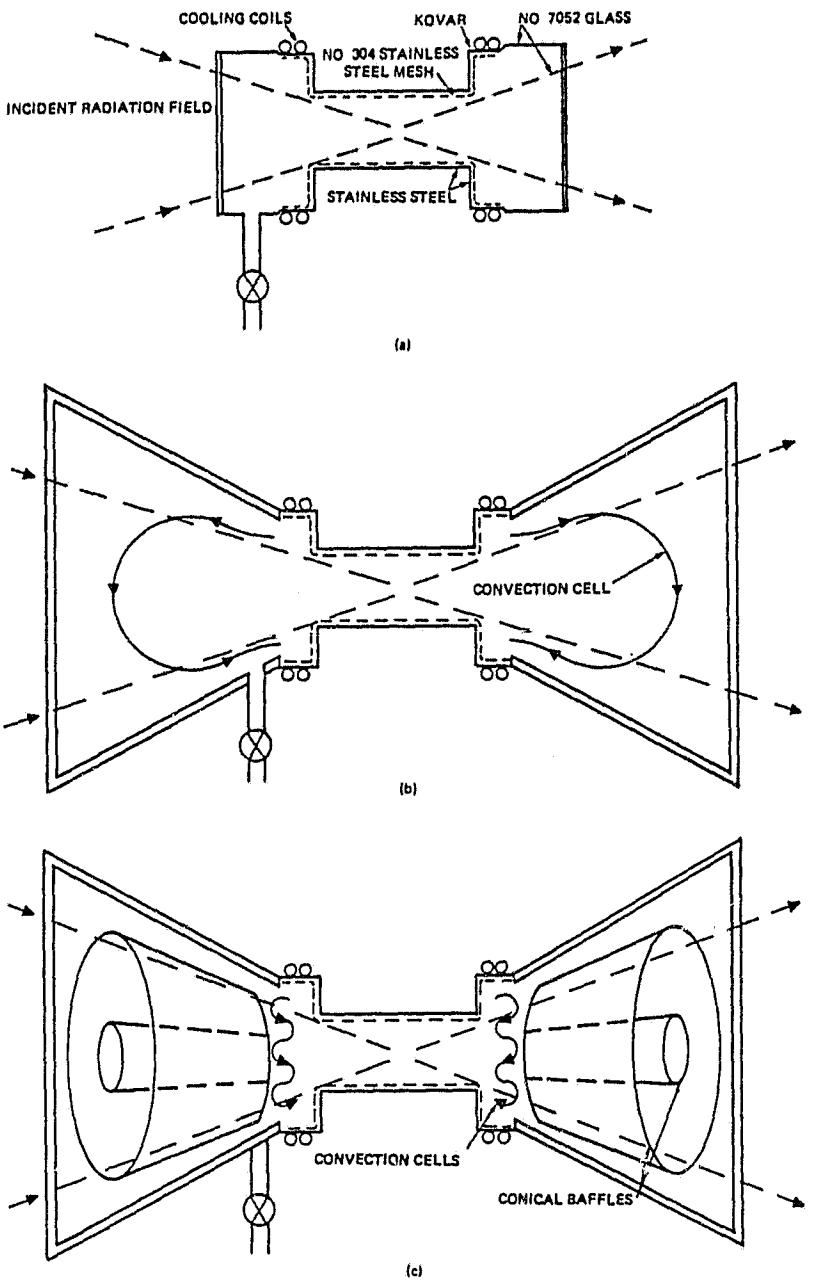

Figure 22. Heat pipe cell design evolution. (a) Earliest - (c) latest.

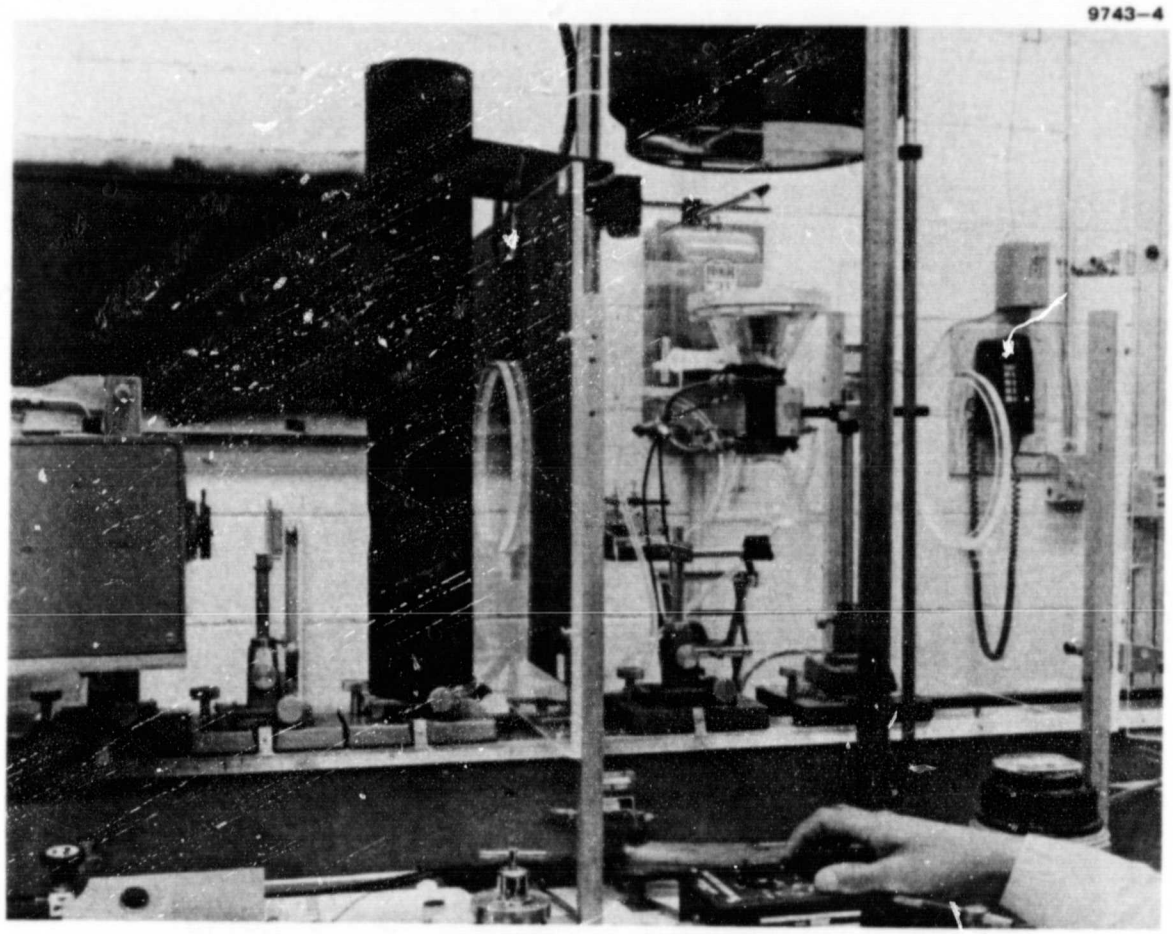

Figure 23. Experimental set-up which demonstrated plasma heating. Solar simulator is at the top, heat pipe cell is at center, and monocrometer is at the left of the photograph.

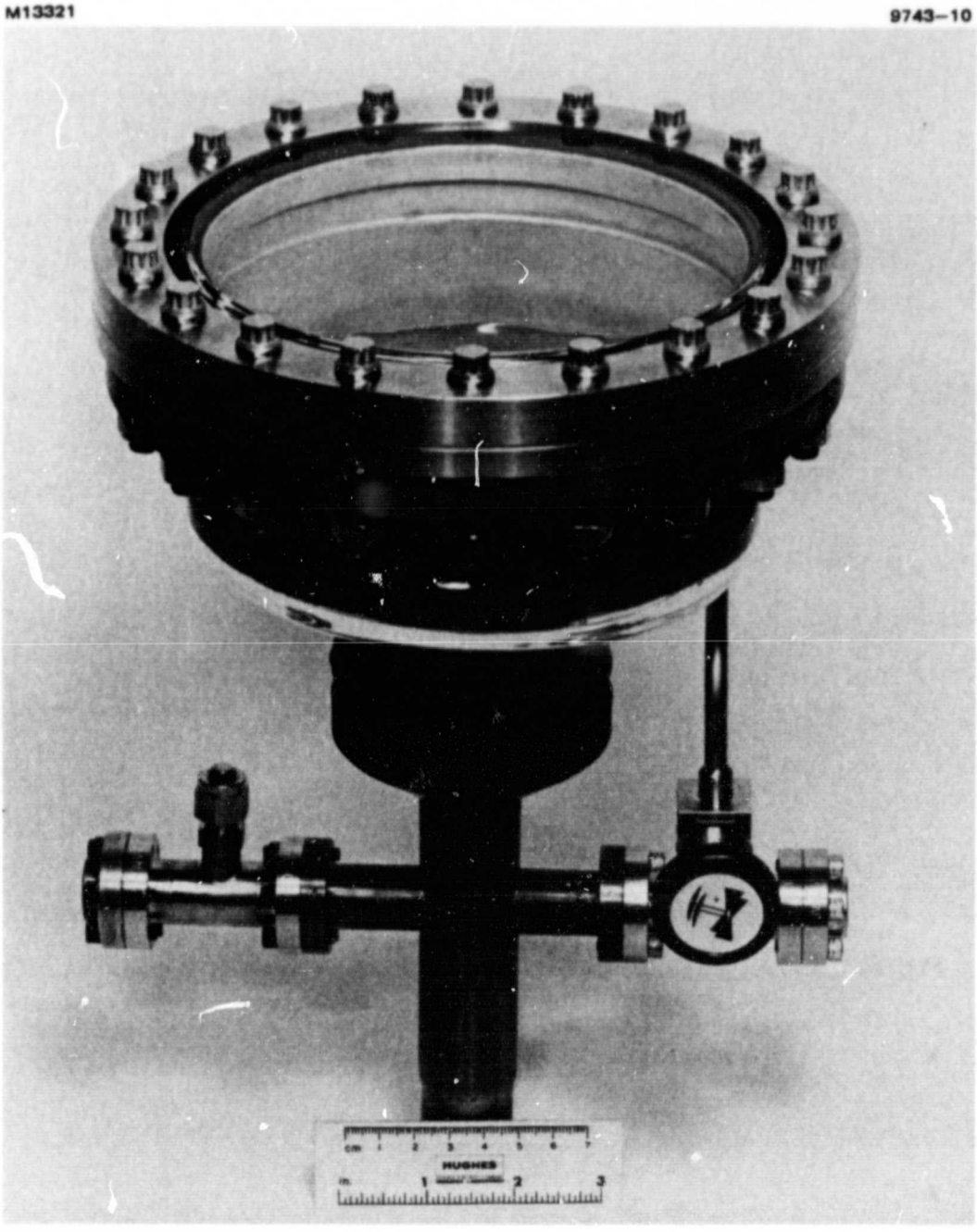

Figure 24. New heat pipe cell with transverse viewing ports.

13300 9740-11

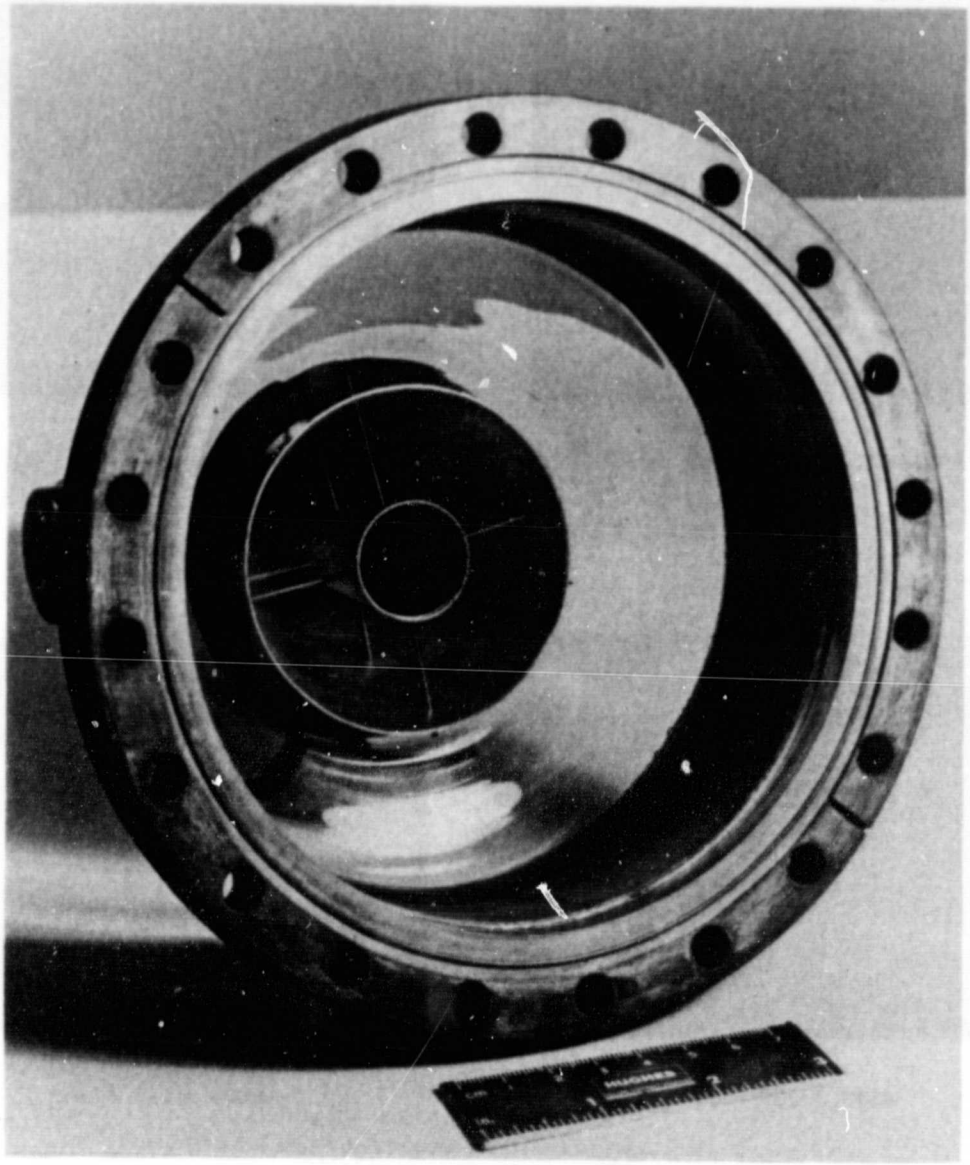

Figure 25. New heat pipe cell showing conical baffles.

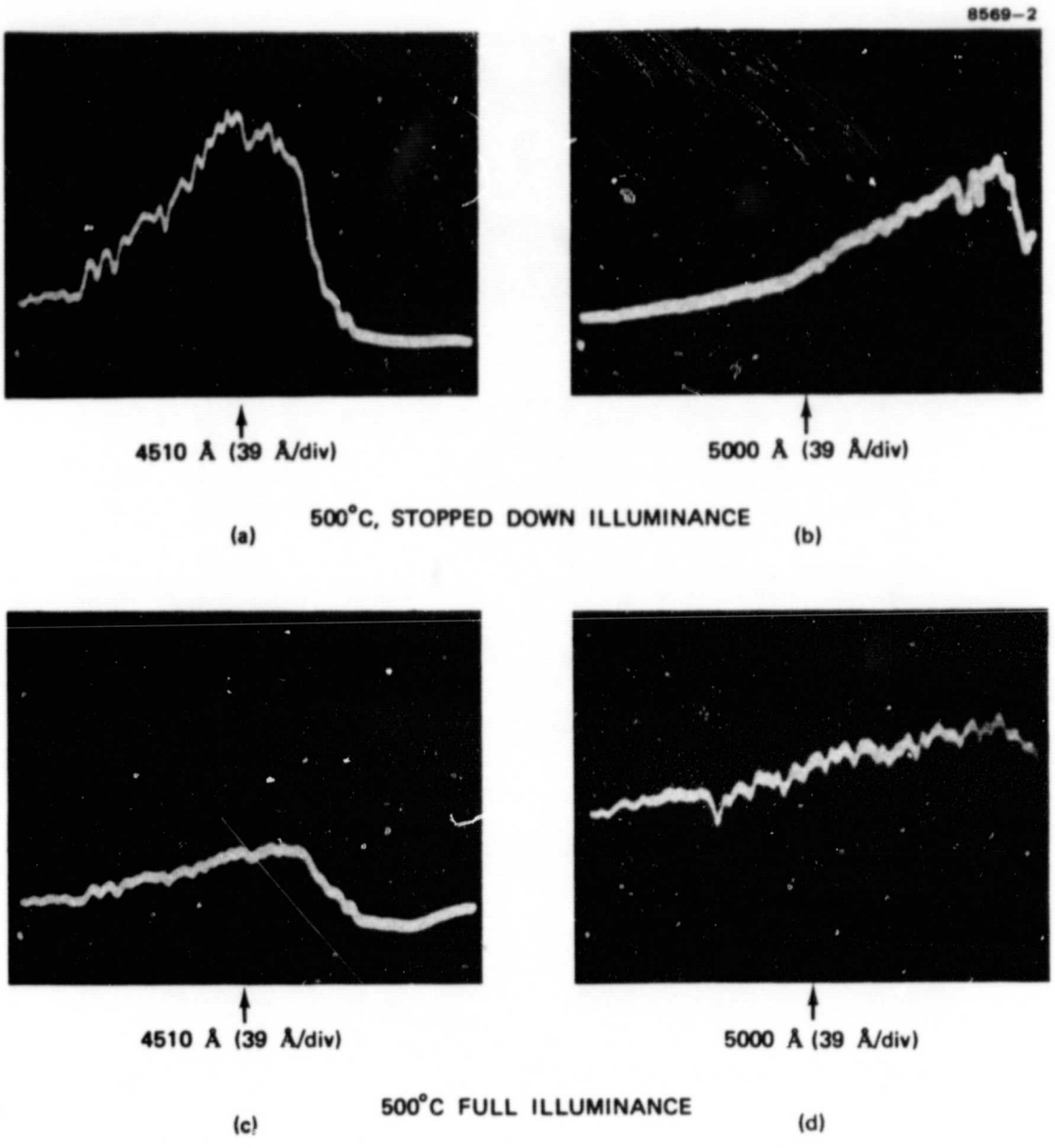

Figure 26. High-temperature cesium absorption spectra under partial illumination from the solar concentrator (a,b) and under full ∿377-W illumination by the concentrator (c,d).

function of wavelength evident at full illuminance indicate thermal dissociation of the dimer ground state caused by heating of the incident radiation field. Window fogging problems prohibited any quantitative interpretation of the data from these experiments.

When the window fogging problem was finally eliminated with the baffled heat pipe cell apparatus shown in Figure 23, three different spectral signatures of plasma heating were observed. An independent result for the plasma temperature was obtained from two of these. The first spectral signature of plasma heating is the reduction of the ground-state dimer absorption caused by thermal dissociation. This is shown in Figure 27. In Figure 27(a), a characteristic dimer absorption band is seen near 6300 Å when the incident solar simulator radiation is attenuated by about a factor of 10^{-3} before entering the plasma cell. Under illumination by unattenuated radiation from the simulator, the Figure 27(b) results show that the absorption strength on these bands has been reduced by at least 90%. The associated plasma temperatures can be estimated from the absorption strength dependence on dimer concentration and the temperature dependence of the equilibrium fraction of dimers:

$$\frac{I}{I_o} = \exp\left(-\sigma L\,[Cs_2]\right) \tag{26}$$

$$[Cs_2] = K\,[Cs]^2 \tag{27}$$

$$[Cs] = [Cs]_o\,(T_o/T) \quad , \tag{28}$$

where σ is the absorption cross section, L is the optical path length in the vapor, T_o is the oven temperature, T is the plasma temperature, K is the equilibrium constant, $[Cs_2]$ is the ground-state dimer concentration, and $[Cs]_o$ is the equilibrium monomer concentration at $T = T_o$. In the experiment, $L \simeq 10$ cm, $T_o = 500°C$, $[Cs]_o = 1 \cdot 10^{18}$ cm^{-3}, $K = 1.3 \cdot 10^{-23} \exp(5237/T)$ cm^3, and σ ($\lambda = 6300$ Å) $= 1 \cdot 10^{-16}$ cm^2 (see

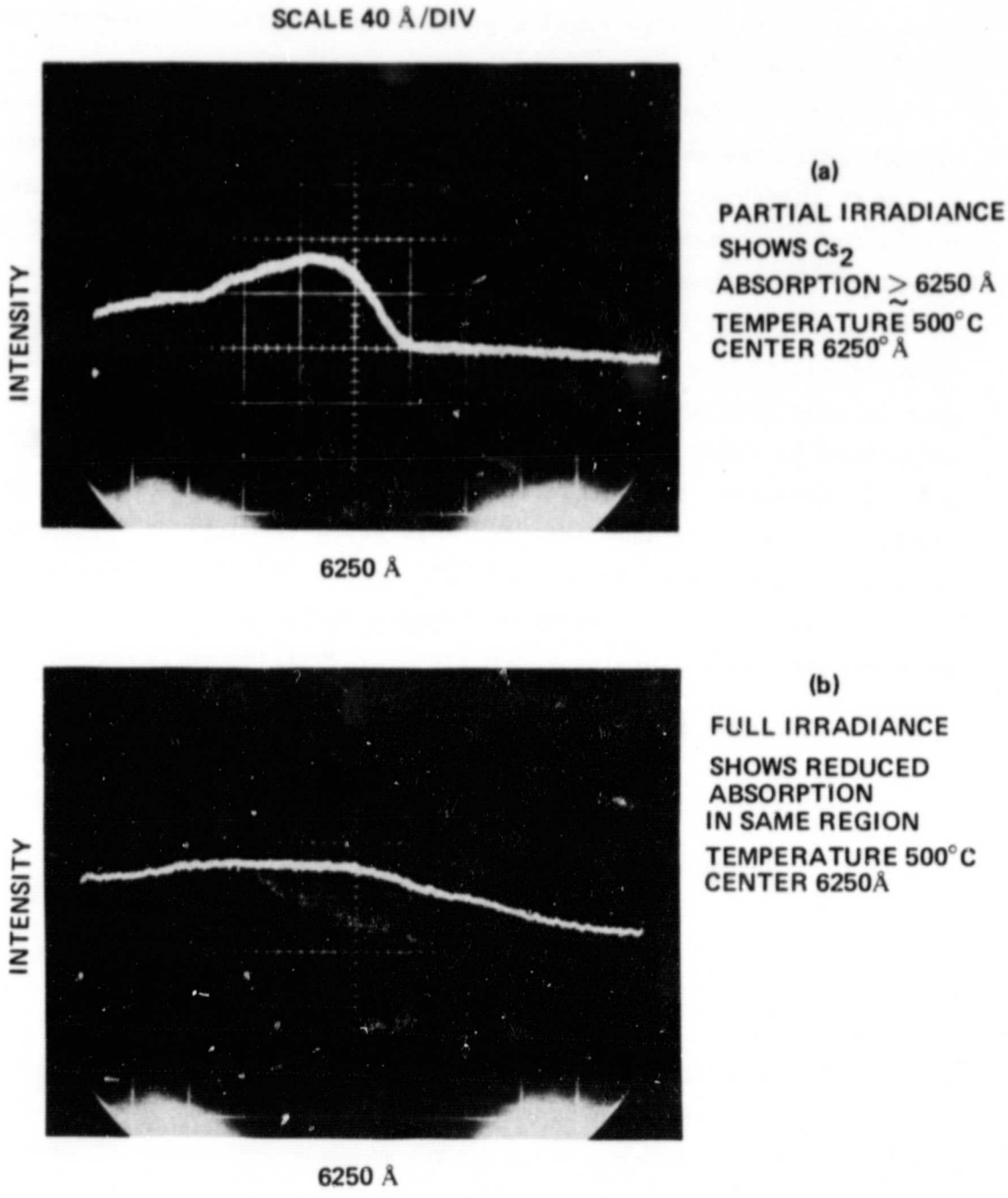

Figure 27. Plasma formation signatures: dimer dissociation.

Figure 1). From the data in Figure 25, I/I_o (6300 Å) $\gtrsim 0.9$ within the experimental error. This implies

$$T > 1528°K \quad . \tag{29}$$

The second spectral signature of plasma heating is shown in Figure 28, together with a reference cesium lamp emission spectrum. The absorption lines present in the plasma cell spectrum at 6723 Å and 6973 Å are due to the $7d^2D \rightarrow 6p^2P$ transitions on the monomer, illustrated in Figure 29. Thus, the absorption dips are a direct indication that the resonance level of cesium is populated. The absorption cross section for these lines is given by

$$\sigma = \frac{\lambda^3}{4\pi^2 c}\left(\frac{\lambda}{\Delta\lambda}\right) A \quad . \tag{30}$$

The A coefficient is estimated as $A \simeq 12 \cdot 10^6$, and $\Delta\lambda$ from the spectra is $\sim$10 Å. These give

$$\sigma \simeq 2.2 \cdot 10^{-15} \text{ cm}^2 \quad . \tag{31}$$

The population of the $6p^2P$ resonance level can be estimated from

$$I/I_o = \exp(-\sigma[Cs6p^2P]L) \quad . \tag{32}$$

With L = 10 cm, as before, and $I/I_o \simeq 0.86$, we estimate

$$[Cs6p^2P] \simeq 6.8 \cdot 10^{12} \text{ cm}^3 \quad . \tag{33}$$

The temperature, assuming a Boltzmann population distribution (which is valid at these densities), can be estimated from

$$[Cs6p^2P] = 3[Cs_o](T_o/T) \exp\{-1.4/T(eV)\} \quad , \tag{34}$$

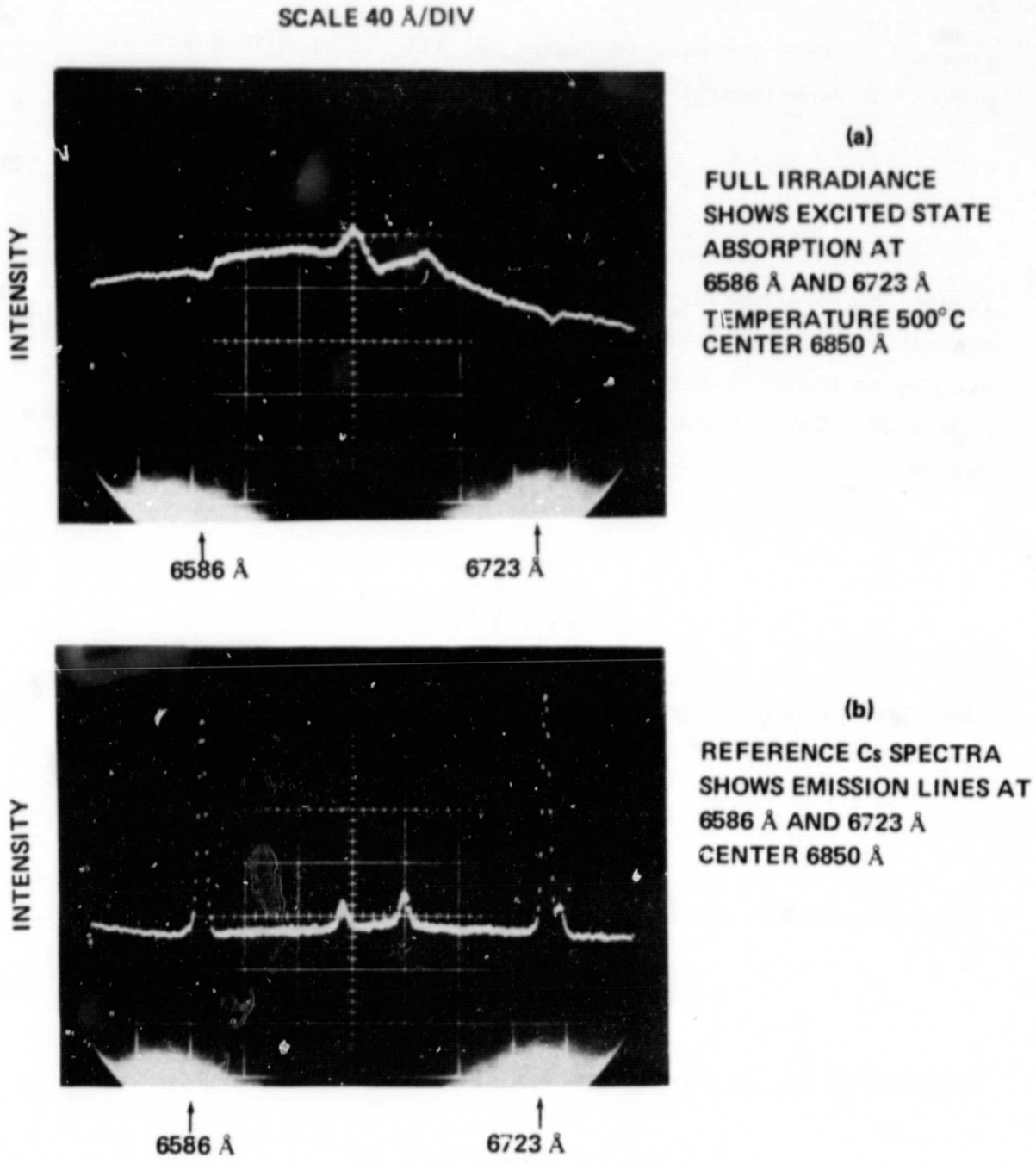

Figure 28. Plasma formation signatures: excited state absorption.

where the factor of 3 is the appropriate degeneracy factor. This gives a temperature estimate of

$$T \simeq 1320°K \tag{35}$$

The third spectral signature of plasma heating is the emission seen at the 8523-Å resonance line as well as the emission seen at 8761 Å from the $6d^2D \rightarrow 6p^2P$ transition shown in Figure 30. The latter emission indicates population of a level at 2.8 eV (see Figure 29). The incomplete knowledge of the effective solid angle of the plasma emission restricts us to simply stating that the above calculated values of the plasma temperature are consistent with the emission strengths observed on these lines.

We were able to compare these temperature estimates with the plasma temperature predicted by the theoretical model under our experimental conditions. Measurements of the incident radiation flux from the solar simulator in the focal volume of the baffled heat pipe cell in these experiments are shown in Figure 31. The power density is seen to be reduced by the baffles to $\sim$20 W/cm^2, with the focal region degraded to about a 2 cm diameter spot. At this power level, dimensional scale and oven temperature ($\sim$500°C) theory predicts that the energy loss from the plasma is dominated by radiation. The radiative energy balance results of Figure 7 predict a plasma temperature of $\sim$1800°K under these conditions.

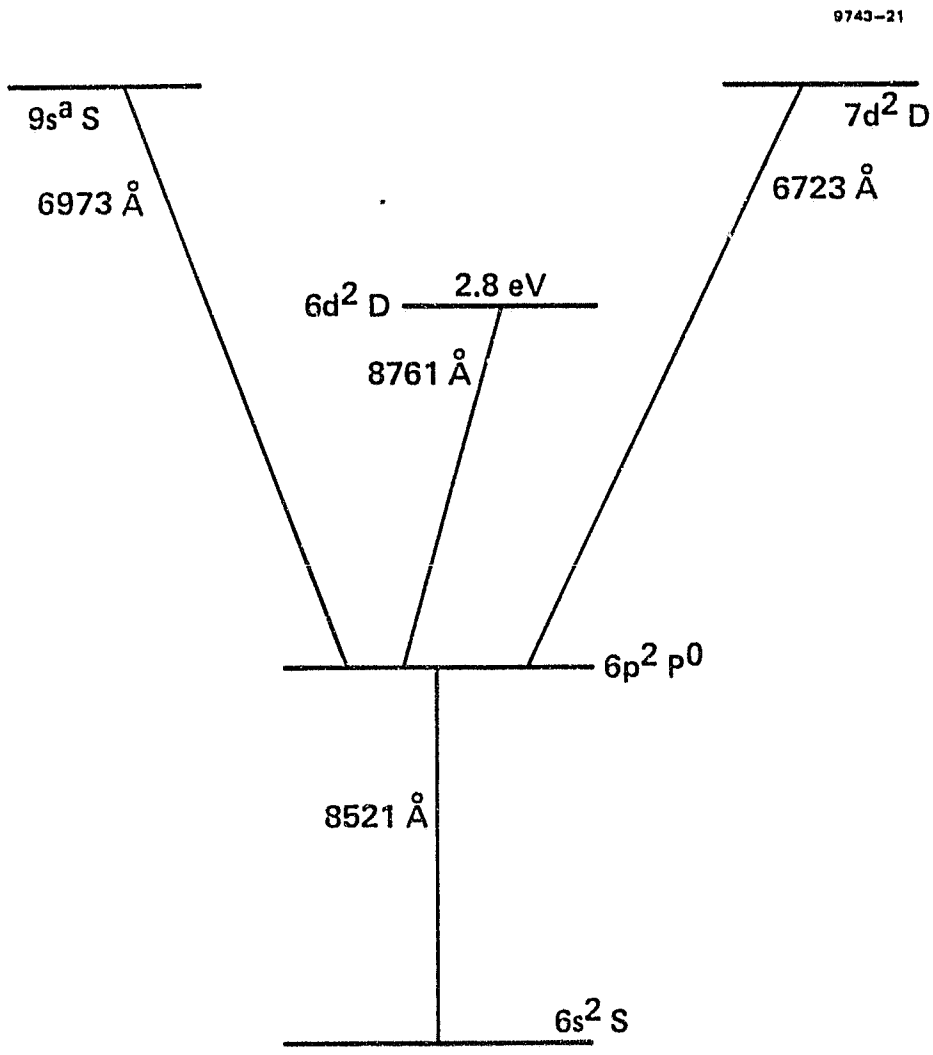

Figure 29. Cesium allowed transitions.

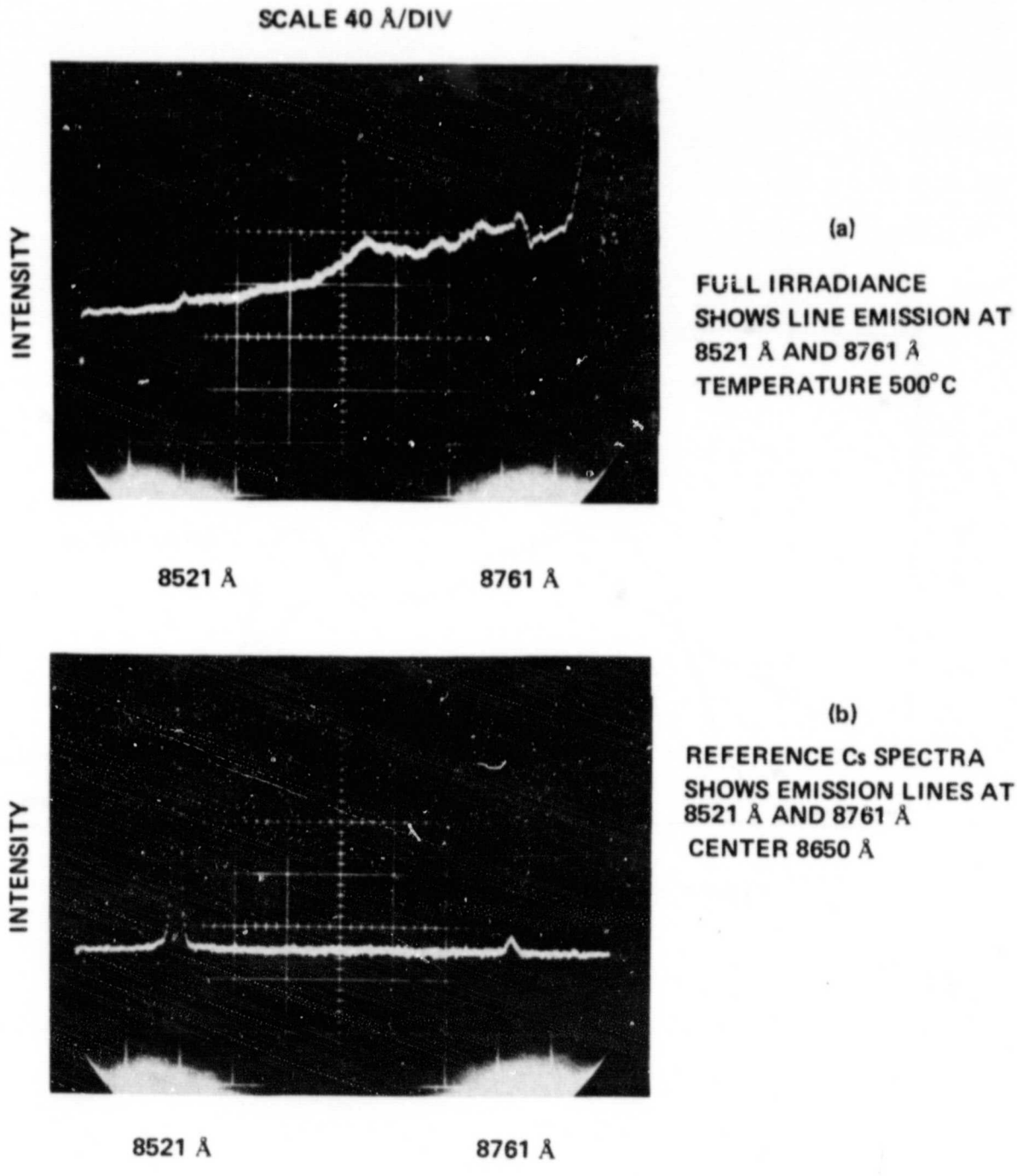

Figure 30. Plasma formation signatures: line emission.

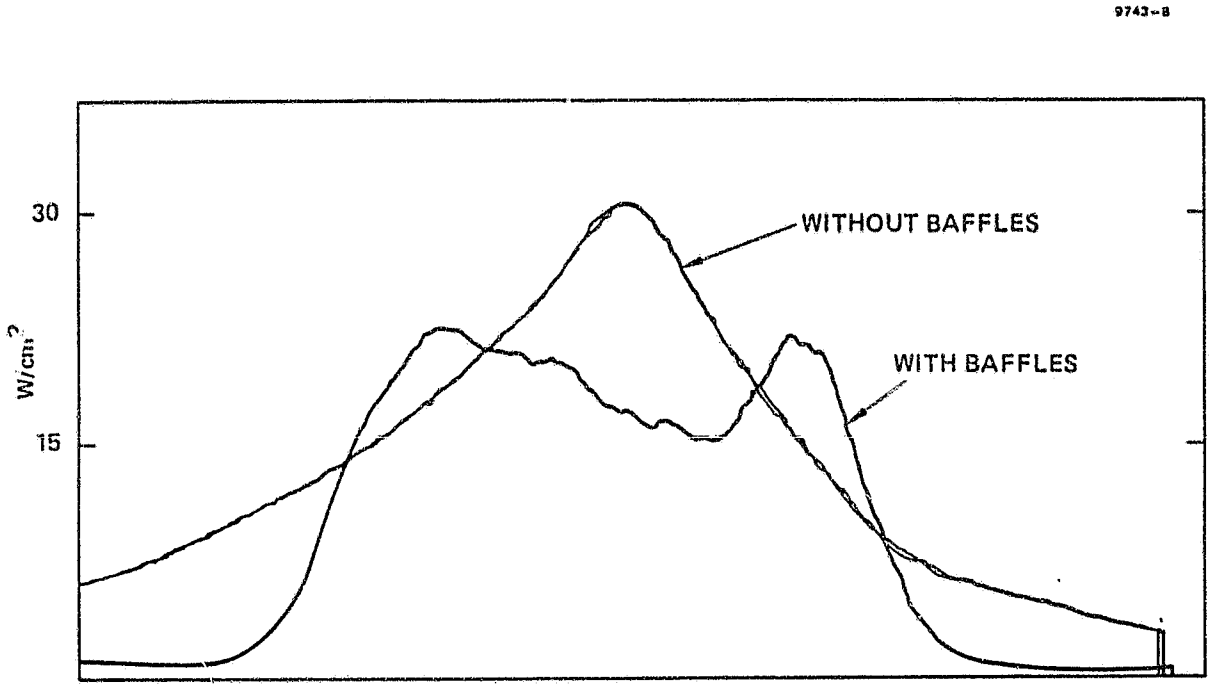

Figure 31. Focal volume irradiance profiles by the solar simulator.

SECTION 4

CONCLUSIONS

The theoretical value of 1800°K for the temperqture predicted to result from heating cesium vapor by the solar simulator represents good agreement with the two experimental measurements of the temperature considering the difference of the xenon arc lamp spectra from the assumed black body form and uncertainties of the effective optical paths through the focal volume. This agreement confirms the predictive power of the model and establishes increased confidence in our prediction that a plasma temperature of ∿2800°K will result when the cell is illuminated with sunlight concentrated by the Fresnel lens to ∿300 W/cm^2.

Thus, solar-driven MHD remains an extremely attractive approach to the generation of electric power in space, potentially representing an orders-of-magnitude improvement in cost and weight factors compared to photovoltaic for large-scale power production.

There are three well-defined research milestones that now remain in order to bring the high-temperature solar MHD converter concept to the stage of an operating solar electric generator. The first is an experimental confirmation of our theoretical prediction that an ∿2800°K plasma temperature can be reached through heating cesium vapor by sunlight concentrated to ∿300 W/cm^2 by a Fresnel lens. The second milestone is the establishment of a theoretical model of the complete solar-heated-plasma MHD cycle with which efficiency and weight optimization studies can be carried out. Finally, the third milestone is the design and fabrication of a prototype high-temperature solar MHD electric generator.

REFERENCES

1. J. Klepeis and V. Hruby, Proc. Engineering Aspects of a MHD (1977) p. I.5.31.

2. D. Eliot, Jet Propulsion Laboratory, and E. Pierson, Argonne Nat. Laboratory, Personal Communication and papers by same authors at Symposia on Engineering Aspects of MHD through 1980.

3. A.J. Palmer, Prog. in Astronautics & Aeronautics 61, 201 (1978).

4. A.T. Mattick, Prog. in Astronautics & Aeronautics 61, 159 (1978).

5. A.J. Palmer, "Radiatively Sustained Plasmas for Solar Electric Conversion," 1st Annual Technical Report, Contract NAS 2-10001, August 1979.

6. A.J. Palmer, "Modeling of a Solar Pumped MHD Excimer Laser," Appl. Phys. (in press).

7. A.J. Palmer and G.J. Dunning, Bulletin American Phys. Soc. 25, No. 4. Paper A.J. 14, p. 494, April (1980). A.J. Palmer and G.J. Dunning, "Radiatively Sustained Cesium Plasmas for Solar Electric Conversion," Final Technical Report for Contract NAS 2-10001, July 1980.

8. Ya.B. Zel'dovich and Yu.P. Raizer, Physics of Shock Waves and High Temperature Hydrodynamic Phenomena, Vol. 1, Academic Press, N.Y., 1966.

9. R.E.M. Hodges, D.L. Drummond, and A. Gallagher, Phys. Rev. A, 1519 (1972).

10. A.J. Palmer, J. Appl. Phys. 47, 3088 (1976).

11. R. Rodgers, N. Krascella, and J. Kendall, Final Technical Report, Contract NAS 2-10019, February 1979, "Solar Sustained Plasma."

12. G. Herzberg, Spectra of Diatomic Molecules, (Van Nostrand, New York, 1950, Appendix.

13. A.E. Wechsler, "Characteristics of Metal Vapor," Arthur D. Little, Inc., Cambridge, MA, Aerospace Research Laboratories Report ARL 66-004, Jan. 1966.

14. J.F. Weymouth, J. Inst. of Elect. Eng. 8, 38-0, August 1962.

15. L.K. Hanson and N.S. Rasor, Proc. of 2nd NASA Conf. on Laser Energy Conversion, Jan. 1975, p. 133.

16. A. von Engel, Ionized Gases (Oxford Press, 1965).

17. B.C. Lindley, Proc. Engineering Aspects of MHD (1960), p. 177.

18. R.J. Rosa, A. Kantrovitz, Direct Conversion of Heat to Electricity, J. Kage and J. Welsh, Eds. (Wiley, 1960).

19. American Institute of Physics Handbook, McGraw-Hill, 1963.

20. W. Vincenti and C. Kruger, Introduction to Physical Gas Dynamics, John Wiley & Sons, New York, 1965.

21. "Radiatively Sustained Cesium Plasmas for Solar Energy Conversion, Hughes Research Laboratories Technical Proposal No. 78M-0201/E2692, February 1978.

22. The CsXe potential curves are from J. Pascale and J. Vandeplanque, CEA Report March 1974. The Cs_2 curves are from R.P. Benedict, D.L. Drummond and L.A. Schlie, J. Chem. Phys. 66, No. 10, 4600 (1977).

23. H. Horwitz, Jr., G.W. Sutton, and S. Tamor, ARS Journal 32, 1237 (1962).

24. B. Zanderer, E. Tate, and C.H. Marston, "CO_2 MHD Laser; Analysis, Design and Shock Tunnel Experiments," Proc. 14th Symposium on Engineering Aspect of MHD.

25. A.J. Palmer, L.D. Hess, et al., "Excimer Lasers," Final Report, NASA Contract NAS 3-19707, November 1977.

26. P.G. Burke and A.J. Taylor, J. Phys. B: Atom. Molec. Phys. 2, 869 (1969).

27. C. York and A. Gallagher, Jr., Inst. Lab. Astrophys. Report 114, October 1974.

28. A.C. Gallagher and A.V. Phelps, Final Technical Report. ERDA Contract No. E(49-1)-3800, February 1977.

29. Electron collisional de-excitation and dissociation may depress the dimer gain even further. This was the case in the modeling of previous static-discharge-pumped alkali systems.[25,28] An accurate assessment of the influence of electron collisional deactivation of the dimer A state must await a more complete numerical model since it depends sensitively on the dissociative recombination and multistep ionization rates. Electron deactivation is not expected to affect the excimer gain because of the high heavy particle dissociation rate controlling the population of the excimer A state.

30. The low Mach number equilibrium regime is essentially the same kinetic regime that was explored previously with static discharges through alkali-rare gas mixtures.[25,28] The absorption due to the equilibrium concentration of ground state dimers was at the root of the failure to achieve laser action in these experiments.

31. C.K. Vidal and J. Cooper, J. Appl. Phys. 40, 3370 (1969).

APPENDIX

FLOW CHART FOR SOLAR SUSTAINED PLASMA MODEL